Rnd2 differentially regulates oligodendrocyte myelination at different developmental periods

Yuki Miyamoto[a,b,*], Tomohiro Torii[c], Miho Terao[d], Shuji Takada[d], Akito Tanoue[a], Hironori Katoh[e], and Junji Yamauchi[a,b,*]

[a]Department of Pharmacology and [d]Department of Systems BioMedicine, National Research Institute for Child Health and Development, Setagaya, Tokyo 157-8535, Japan; [b]Laboratory of Molecular Neuroscience and Neurology, Tokyo University of Pharmacy and Life Sciences, Hachioji, Tokyo 192-0355, Japan; [c]Laboratory of Ion Channel Pathophysiology, Graduate School of Brain Science, Doshisha University, Kyotanabe, Kyoto 610-0394, Japan; [e]Laboratory of Molecular Neurobiology, Graduate School of Pharmaceutical Sciences, Kyoto University, Sakyo, Kyoto 606-8501, Japan

ABSTRACT **In the CNS, oligodendrocyte precursor cells differentiate into oligodendrocytes to wrap their plasma membranes around neuronal axons, generating mature neural networks with myelin sheaths according to spatial and temporal patterns. While myelination is known to be one of the most dynamic cell morphological changes, the overall intrinsic and extrinsic molecular cues controlling myelination remain to be fully clarified. Here, we describe the biphasic roles of Rnd2, an atypical branch of the Rho family GTPase, in oligodendrocyte myelination during development and after maturation in mice. Compared with littermate controls, oligodendrocyte-specific Rnd2 knockout mice exhibit decreased myelin thickness at the onset of myelination but increased myelin thickness in the later period. Larger proportions of Rho kinase and its substrate Mbs, the signaling unit that negatively regulates oligodendrocyte myelination, are phosphorylated at the onset of myelination, while their smaller proportions are phosphorylated in the later period. In addition, we confirm the biphasic role of Rnd2 through experiments with oligodendrocyte-specific Rnd2 transgenic mice. We conclude that Rnd2 positively regulates myelination in the early myelinating period and negatively regulates myelination in the later period. This unique modulator thus plays different roles depending on the myelination period.**

Monitoring Editor
Terry Lechler
Duke University

Received: May 26, 2020
Revised: Feb 2, 2021
Accepted: Feb 11, 2021

This article was published online ahead of print in MBoC in Press (http://www.molbiolcell.org/cgi/doi/10.1091/mbc.E20-05-0332) on February 17, 2021.

Conflict of interest: The authors declare no competing financial interest.

Author contributions: Y.M. and J.Y. designed the experiments and wrote the manuscript. Y. M. conducted the majority of the experiments. T.T. prepared the genetically modified mice required for the experiments. M.T. and S.T. generated the transgenic mice. A.T. and H.K. acquired unpublished data.

*Address correspondence to: Yuki Miyamoto (miyamoto-y@ncchd.go.jp); Junji Yamauchi (yamauchi@toyaku.ac.jp).

Abbreviations used: ANOVA, analysis of variance; CNPase, 2′, 3′-cyclic-nucleotide 3′-phosphodiesterase); CNS, central nervous system; DIV, day in vitro; DRG, dorsal root ganglion; FGF, fibroblast growth factor; GAP, GTPase-activating protein; GDP, guanosine diphosphate; GEF, guanine-nucleotide exchange factor; GFAP, glial fibrillary acidic protein; GTP, guanosine triphosphate; GTPase, guanosine triphosphatase; LINGO-1, leucine-rich repeat and immunoglobulin-like domain–containing Nogo receptor-interacting protein-1; MBP, myelin basic protein; NF, neurofilament; OPCs, oligodendrocyte precursor cell; PBS, phosphate-buffered saline; PDGFR, platelet-derived growth factor receptor; PFA, paraformaldehyde; PI3K, phosphatidylinositol-3 kinase; PTEN, tensin homologue deleted from chromosome 10; TSC1/2, tuberous sclerosis complex 1/2.

INTRODUCTION

During the development of the CNS, oligodendrocyte precursor cells (OPCs) arise along the caudorostral axis of the ventricular neuroepithelium (Bradl and Lassmann, 2010; Simons and Lyons, 2013; Bergles and Richardson, 2015; Saab and Nave, 2017). OPCs then differentiate into mature oligodendrocytes, forming myelin sheaths with their multiple layers. Mature myelin sheaths protect axons from various external stresses, including physical and physiological stresses, and insulate them to increase nerve conduction velocity. Although we know of various extrinsic and intrinsic cues such as growth factors, cell adhesion molecules, and protein kinases that mediate cellular morphology and gene expression, thereby regulating the spatial and temporal patterns of oligodendrocyte myelination, the overall picture of the myelination mechanism remains to be thoroughly clarified (Zuchero and Barres, 2013).

Myelin formation begins with the first contact of oligodendrocyte processes along axons, which triggers the subsequent steps. The molecular steps controlling oligodendrocyte myelination often involve the extensive reorganization of cytoskeletal proteins, leading to morphological changes (Nawaz *et al.*, 2015;

Zuchero *et al.*, 2015). The small guanosine triphosphatase (GTPase) family is a major regulator underlying such changes. It serves as a molecular switch by cycling between an active guanosine triphosphate (GTP)-bound form and an inactive guanosine diphosphate (GDP)-bound form (Jaffe and Hall, 2005; Rossman *et al.*, 2005). In the active state, members of this family bind to downstream effectors to evoke diverse biological functions. For example, Rho family small GTPases Cdc42 and Rac1 act as positive molecular switches controlling oligodendrocyte differentiation and myelination (Liang *et al.*, 2004; Thurnherr *et al.*, 2006). The leucine-rich repeat and immunoglobulin-like domain–containing Nogo receptor-interacting protein (LINGO)-1, a component of the p75 neurotrophin receptor and tumor necrosis factor receptor family member Troy signaling complex, negatively regulates myelination through a RhoA-dependent mechanism (Mi *et al.*, 2004). The inhibition of LINGO-1 leads to the down-regulation of RhoA activity and promotes OPC differentiation in vitro (Zhao *et al.*, 2007).

The Rnd proteins, Rnd1, Rnd2, and Rnd3/RhoE, which constitute a unique branch of the Rho family of small GTPase, are important regulators of cell migration, morphological changes, and differentiation in various types of cells (Chardin, 2006; Riou *et al.*, 2010). Rnd proteins have weak or no intrinsic GTPase activity and accordingly are constitutively bound to GTP. They are thought to be regulated at the expression, phosphorylation, or cellular localization levels. It is likely that Rnd proteins, especially Rnd1 and Rnd3, bind to the p190RhoGAP and increase the GTPase-activating protein (GAP) activity to decrease active GTP-bound RhoA, which antagonizes the cellular functions of RhoA and the downstream Rho kinase (Wennerberg *et al.*, 2003). Rnd2 plays a role in morphological changes in neuronal cells (Fujita *et al.*, 2002; Tanaka *et al.*, 2006) and also induces neurite branching in concert with the effector protein, Rapostlin, in PC12 cells (Fujita *et al.*, 2002). Furthermore, the transcription factor Neurogenin-2 is known to promote the radial migration of cortical neurons by inducing the expression of Rnd2 along the time axis (Heng *et al.*, 2008).

Here, we report that Rnd2 affects oligodendrocyte myelination in different ways during different periods of development. In mice, knockout of Rnd2 in oligodendrocytes leads to decreased myelin thickness in an early developmental period soon after birth but leads to increased myelin thickness in a later developmental period, which is in keeping with the results from oligodendrocyte-neuronal cocultures. The role of Rnd2 can also be observed using oligodendrocyte-specific Rnd2 transgenic mice. These phenomena are consistent with the fact that signaling through Rho kinase occurs in a dephosphorylated state and is down-regulated during the first period of myelination but occurs in a phosphorylated state later in the myelination process. A similar observation was made in the case of Rnd2 knockout in adulthood. Together, our findings reveal that Rnd2 has different effects on the regulation of myelination in different periods of myelination, demonstrating that Rnd2 plays a unique role in the CNS.

RESULTS

Rnd2 is up-regulated during CNS development

Rnd2 is a small GTPase that has been extensively investigated in neuronal progenitor cells (Fujita *et al.*, 2002; Tanaka *et al.*, 2006; Heng *et al.*, 2008). Transcriptome data related to oligodendrocyte differentiation have been reported by our own and other groups (Dugas *et al.*, 2006). Our transcriptome analysis shows that Rnd2 is transcribed in rat primary oligodendrocytes in our transcriptome analysis (Table 1).

To examine the expression patterns of Rnd2 during CNS development, we performed immunoblotting with an anti-Rnd2 antibody using whole mouse brains. The expression levels of Rnd2 were clearly detectable from 14 d after birth (Figure 1A), the approximate time point when active myelination starts in the developing brain. Elevated expression levels of Rnd2 were detected until adulthood. As the mice developed, the expression levels of the myelin marker proteins 2′, 3′-cyclic-nucleotide 3′-phosphodiesterase (CNPase) and myelin basic protein (MBP), the major central myelin proteins, were increased. The expression levels of control actin were comparable in all stages. The expression profiles of Rnd2 and myelin marker proteins in cocultures established from the primary oligodendrocytes and dorsal root ganglion (DRG) neurons (1–21 d in vitro [DIV]) of rats were similar to those observed in developing brains (Figure 1B). Additionally, in immunoblotting using lysates from primary oligodendrocytes, the expression levels of Rnd2 were detected from DIV1 and increased as differentiation proceeded (Figure 1C). Similar patterns were observed in myelin marker proteins. These results suggest that Rnd2 is progressively expressed in differentiating oligodendrocytes and that its expression increases as myelination proceeds in the CNS.

During development, OPCs undergo a differentiation program that is traced by myelin-specific expression markers and typical changes in cell morphology. To further characterize the spatial and temporal expression of Rnd2, we performed immunohistochemical analysis using mouse brain sections. Rnd2 exhibited a dispersive expression in tissues and was costained with the platelet-derived growth factor receptor (PDGFR) α-positive oligodendrocyte precursor cells at postnatal day 7 and the premyelinating marker O4 at postnatal day 14 as well as with the myelinating oligodendrocyte marker CC1 at postnatal days 14 and 21 in the corpus callosum (Figure 1, D and E). In addition, immunostaining of the corpus callosum at postnatal day 14 using an antibody against neurofilament (NF) proteins revealed that Rnd2 was not present in NF-positive cells (Figure 1F).

Rnd2 regulates the onset of myelination

Next we investigated the effect of knockout of Rnd2 in oligodendrocytes. We generated Rnd2 conditional knockout mice that were suitable for the Cre-loxP recombination system (Figure 2A). Oligodendrocyte-specific MBP promoter–driven Cre recombinase transgenic mice were used for the deletion of loxP-flanked genes. Production of Rnd2 conditional knockout mice was confirmed by Southern blotting (Supplemental Figure S1A) and genomic PCR (Supplemental Figure S1B) with specific probes and primers, respectively, using tail genomic DNA. To check whether Cre was active in MBP promoter–expressing tissues, we designed the primer pair for the Cre-excised region and performed PCR amplification using the genome from the mouse corpus callosum (Supplemental Figure S1C). To further confirm knockout effectiveness in the mouse brain, we preformed coimmunostaining for Rnd2 with CC1 in the corpus callosum. Staining for Rnd2 was decreased in knockout mice (Supplemental Figure S1, D and E).

We first performed an immunohistochemical analysis of MBP in 14-d-old brain tissues. Knockout of Rnd2 decreased MBP staining levels compared with littermate controls (Figure 2, B and C, tentatively referred to as *Rnd2*$^{fl/fl}$*; Mbp-Cre* in the figure panels). The number of cells positive for the oligodendrocyte lineage cell marker Olig2 was unchanged in knockout mice (Figure 2, B and D). Staining for the astrocyte marker glial fibrillary acidic protein (GFAP) and the neuron marker NeuN was comparable between knockout mice and controls (Supplemental Figure S2, A–D). Recently, CNPase has been shown to be crucial for maintaining key channels in the myelin sheaths. An increase in CNPase has

Order	GenBank Acc. No.	Name	Sample 1		Sample 2		Sample 3		Sample 1	Sample 2	Sample 3	
			Day 0	Day 3	Day 0	Day 3	Day 0	Day 3	Log2 (ratio)	Log2 (ratio)	Log2 (ratio)	*P* value
1	NM_001025291.1	Mbp	17	21566	64	10924	42	19323	10.27	7.41	8.86	0.006
2	NM_017190.4	Mag	3	1247	6	649	3	1445	8.59	6.83	8.72	0.010
3	NM_013161.1	Pnlip	14	3645	94	3991	62	4016	8.00	5.41	6.02	0.000
4	NM_030990.1	Plp1	65	15902	88	5920	61	10702	7.94	6.07	7.44	0.020
5	NM_053457.2	Cldn11	28	6210	74	4370	163	9306	7.80	5.88	5.84	0.011
6	NM_001107967.2	Tmem125	1	149	2	106	1	351	6.68	5.82	8.01	0.057
7	NM_001107311.1	Enpp6	5	408	5	279	4	621	6.34	5.67	7.15	0.012
8	XM_008773131.2	Shroom2	15	940	26	440	18	539	5.95	4.07	4.93	0.015
9	NM_001108598.2	Dusp15	3	164	9	210	10	378	5.90	4.58	5.19	0.020
10	NM_198754.2	Cmtm8	10	529	13	282	19	334	5.73	4.46	4.12	0.008
11	NM_012827.2	Bmp4	16	802	49	1145	60	570	5.68	4.56	3.25	0.009
12	NM_022668.2	Mog	5	228	5	249	4	618	5.63	5.72	7.35	0.046
13	NM_053936.3	Edg2	12	386	15	171	14	439	4.98	3.55	5.02	0.018
14	XM_001057493.1	Plxnb3	18	566	24	340	32	601	4.96	3.80	4.24	0.004
15	NM_001107558.1	Nkx6.2	5	162	12	220	14	458	4.92	4.19	5.06	0.041
16	NM_001110763.1	Tmem163	11	302	26	337	14	591	4.79	3.72	5.38	0.013
17	NM_019276.3	Ugt8	19	522	26	218	20	571	4.79	3.09	4.81	0.020
18	NM_001013434.1	Rras2	48	1274	89	633	36	804	4.72	2.83	4.49	0.012
19	NM_172030.1	Entpd2	19	452	91	748	69	537	4.59	3.05	2.96	0.005
20	NM_001106413.1	Card6	11	255	15	140	10	388	4.58	3.25	5.35	0.026
21	NM_001010953.1	Rnd2	145	3086	447	4442	542	4474	4.42	3.31	3.04	0.002
22	NM_022589.1	Tspan2	64	1328	61	521	69	827	4.38	3.10	3.59	0.024
23	NM_001033757.1	Cdkn1c	21	419	40	395	58	702	4.34	3.32	3.59	0.009
24	NM_032084.1	Chn2	20	373	28	364	14	432	4.21	3.73	4.94	0.000
25	NM_001106610.1	Hdac11	16	265	44	208	26	342	4.07	2.24	3.74	0.004
26	NM_001008368.1	Sirt2	230	3445	352	3636	338	6238	3.90	3.37	4.21	0.010
27	NM_031238.1	Sh3gl3	62	928	151	1051	110	1018	3.89	2.80	3.20	0.000
28	XM_001074337.1	Stmn4	193	2766	245	2419	332	4355	3.84	3.31	3.71	0.008
29	NM_001037773.2	Cyclin J-like	13	181	11	139	15	200	3.80	3.70	3.71	0.001
30	NM_001107277.1	Lgi3	12	161	20	164	36	305	3.78	3.01	3.08	0.018
31	NM_024364.2	Hr	35	461	59	351	67	162	3.73	2.58	1.28	0.037
32	NM_138915.1	Drd1ip	37	453	47	373	65	443	3.61	2.99	2.77	0.000
33	NM_145670.4	Bcas1	109	1290	110	1105	127	1199	3.56	3.33	3.24	0.000
34	NM_001047111.1	Hsmnp1	89	1038	147	944	100	1129	3.55	2.68	3.49	0.000
35	NM_022533.1	Pllp	135	1311	237	609	333	1259	3.28	1.36	1.92	0.024
36	NM_012505.1	Atp1a2	79	749	211	450	94	363	3.25	1.09	1.95	0.034
37	NM_031676.2	Tagln3	40	378	138	450	83	220	3.24	1.71	1.41	0.023
38	NM_001108795.1	Tomoregu-lin-2	67	627	111	279	82	905	3.22	1.32	3.47	0.047
39	XM_217247.4	Mucin 7	43	396	29	243	29	276	3.21	3.05	3.24	0.004
40	NM_012809.1	Cnp1	1425	13014	2271	12426	3373	18736	3.19	2.45	2.47	0.004

TABLE 1: Transcriptome analyses of top 50 mRNAs up-regulated in differentiating rat primary oligodendrocytes and astrocyte markers.

(Continues)

Order	GenBank Acc. No.	Name	Sample 1		Sample 2		Sample 3		Sample 1 Log2 (ratio)	Sample 2 Log2 (ratio)	Sample 3 Log2 (ratio)	*P* value
			Day 0	Day 3	Day 0	Day 3	Day 0	Day 3				
41	NM_012916.2	Bcan	334	2901	710	2532	746	3569	3.12	1.83	2.26	0.002
42	NM_001012345.1	Dgat2	84	722	163	847	182	930	3.11	2.38	2.35	0.001
43	NM_001014011.1	Gramd3	153	1184	385	1201	201	1096	2.96	1.64	2.44	0.000
44	NM_033499.1	Scrg1	448	3474	921	2886	870	2597	2.95	1.65	1.58	0.002
45	NM_001106550.1	Nkain4	47	357	136	589	82	451	2.94	2.11	2.47	0.006
46	NM_080697.2	Dynll2	380	2908	459	3201	385	3864	2.94	2.80	3.33	0.001
47	NM_031648.1	Fxyd1	19	143	102	302	105	270	2.93	1.57	1.36	0.044
48	NM_001013912.1	Mllt11	33	243	25	144	24	164	2.89	2.54	2.79	0.007
49	NM_001024309.1	Taperin	56	413	51	369	84	554	2.88	2.86	2.72	0.003
50	NM_057107.1	Acsl3	349	2376	379	1074	328	1756	2.77	1.50	2.42	0.021
	NM_012988.1	Nfia	21	19	15	7	10	12	–0.14	–1.10	0.26	0.602
	NM_080403.1	Sox9	n.d.	n.d.	n.d.	n.d.	n.d.	n.d.				
	NM_017009.1	gfap	n.d.	n.d.	n.d.	n.d.	n.d.	n.d.				
	NM_001317749.1	aqp4	n.d.	n.d.	n.d.	n.d.	n.d.	n.d.				

Transcriptome analyses were performed using total RNAs from rat primary oligodendrocyte precursor cells before and after the induction of differentiation ($n = 3$ sets of samples; 0 vs. 3 d). The values were sorted by fold increase after differentiation. Effective values are shown in yellow. Astrocyte and oligodendrocyte markers are also shown in green and blue, respectively (n.d., not detected). Those with increasing values, including the *rnd2* gene, which is 21st from the top, are displayed in the logarithm. Comparisons between two groups are shown as *p* values. This table includes differentiating oligodendrocyte markers such as the mRNAs encoding Mbp, Mag, Plp1, Claudin 11 (also called oligodendrocyte-specific protein), Mog, Nkx6.2, and CNPase as well as the oligodendrocyte lineage markers Olig1 and Olig2, but not the mRNAs encoding Nfia, Sox9, Gfap, and Aqp4, which are astrocyte markers.

TABLE 1: Transcriptome analyses of top 50 mRNAs up-regulated in differentiating rat primary oligodendrocytes and astrocyte markers. Continued

been found to be correlated with greater numbers of cytoplasmic channels (Snaidero *et al.*, 2017). Therefore, we next performed immunostaining of CNPase at day 14 in Rnd2 knockout mice. The expression levels of CNPase were decreased in Rnd2 knockout mouse brains (Figure 2, E and F), suggesting a role of Rnd2 in CNPase expression levels. To further confirm the changes in myelin marker expression levels through immunoblotting, we isolated total proteins from brains. Knockout of Rnd2 decreased MBP and CNPase expression levels (Figure 2, G and H), suggesting that Rnd2 is involved in the onset of myelination in vivo.

Because Rnd2 conditional knockout mice exhibited decreased MBP and CNPase levels, we analyzed the myelin ultrastructure in the corpus callosum. Electron microscopic analysis revealed decreased myelin thickness in 15-d-old knockout mice compared with those from control mice (Figure 3A). The decreased myelin thickness in knockout mice is evident from the quantification of the average g-ratios, which are the numerical average ratios of the axon diameter to the diameter of the outermost myelinated fiber. Thinner myelin sheaths with larger average g-ratios as well as distribution of the g-ratios were detected in knockout mice (Figure 3, B–D; 0.864 ± 0.0300 in knockout mice and 0.831 ± 0.0411 in controls).

To further evaluate the role of Rnd2 in myelination, we established an oligodendrocyte-neuronal coculture system. We developed two nonoverlapping Rnd2 short hairpin RNAs (shRNAs; Rnd2#1 and Rnd2#2, which were effective for oligodendrocytes) (Figure 4A). In cocultures, knockdown of Rnd2 in oligodendrocytes decreased the amounts of MBP-positive cells and those of Olig2-positive cells expressing MBP at 21 d (Figure 4, B–D). The amounts of NF proteins were comparable in Rnd2 knocked down cells and controls. Additionally, Rnd2 knockdown decreased the formation of MBP-positive myelin segments and their length (Figure 4, E and F). Similar results were obtained through staining with an anti-CNPase antibody (Supplemental Figure S3, A–C). It seemed likely that Rnd2#2 shRNA was more effective than Rnd2#1 in their length. The number of Olig2-positive cells was not significantly different between control shRNA- and Rnd2 shRNA–infected cocultures (Figure 4G), suggesting that Rnd2 is not essential for the generation of oligodendrocyte lineage cells in vitro. Furthermore, the expression levels of MBP and CNPase were decreased by knockdown of Rnd2 in cocultures (Figure 4, H and I).

Considering these in vivo and in vitro findings together leads us to conclude that Rnd2 is involved in the onset of myelination.

Rnd2 inhibits myelination at later developmental stages

To investigate whether knockout of Rnd2 has the same effects on myelin thickness in later developmental periods, we examined the staining levels of MBP in the 28-d-old brain. It is of note that Rnd2 knockout mice exhibited increased MBP staining levels compared with littermate controls (Figure 5, A and B). In contrast, the number of Olig2-positive cells was unchanged in knockout mice (Figure 5, A and C). These results are consistent with the observable increase in MBP and CNPase levels revealed through immunoblotting (Figure 5, D and E). Additionally, the staining levels of GFAP and NeuN were comparable between knockout and control mice (Supplemental Figure S4, A–D).

Next, we assessed the myelin sheath ultrastructure in 28-d-old knockout mice. Knockout mice exhibited increased myelin thickness compared with controls (Figure 5F). These findings are evident from the quantification of the average g-ratios as well as the distribution

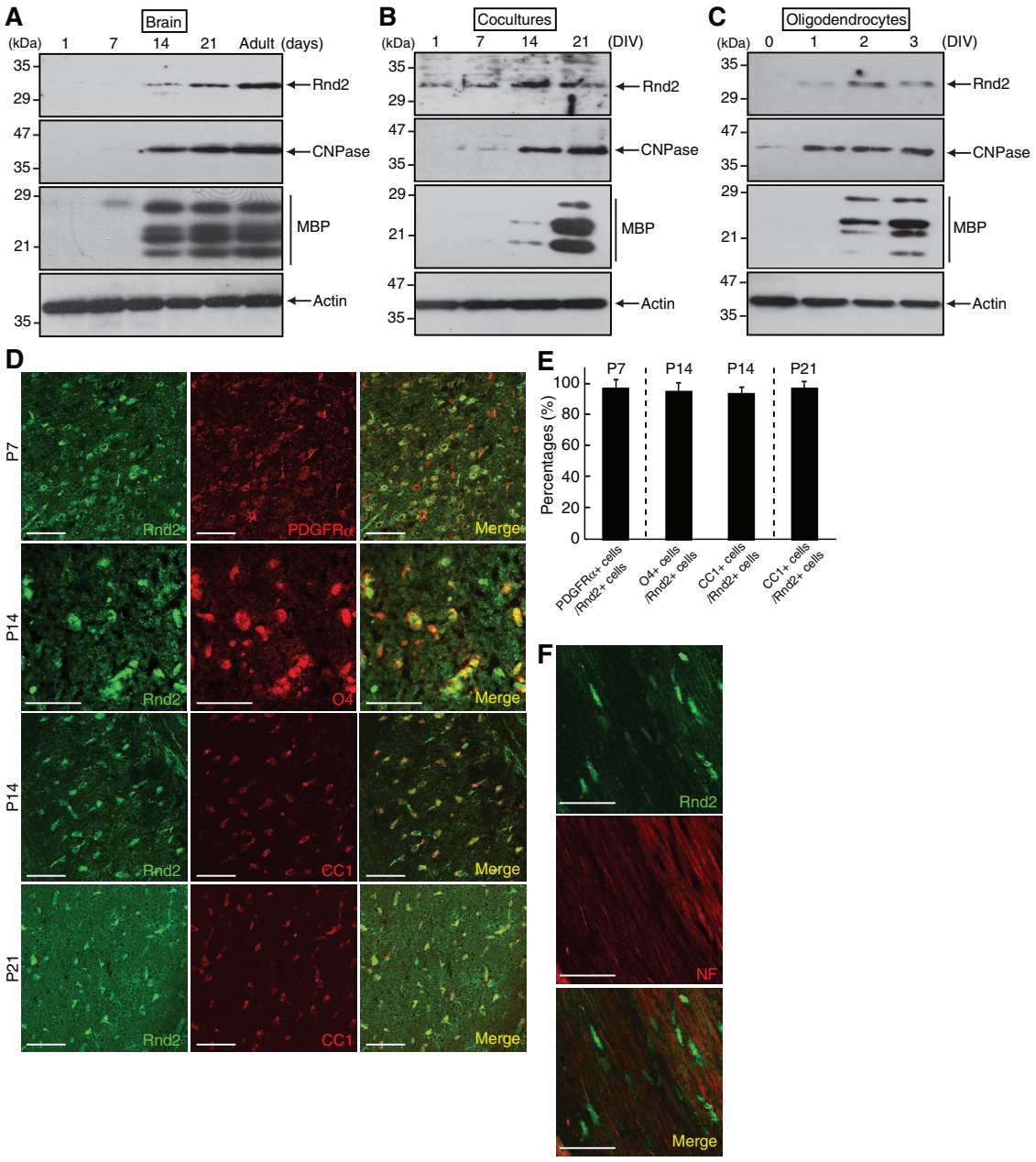

FIGURE 1: Changes in expression levels of Rnd2 and myelin marker proteins. (A) Whole brain tissues from postnatal days 1 to 21 (P1 to P21) and adult stages were isolated, lysed, and used for immunoblotting with the respective antibodies for Rnd2, CNPase, MBP, and control actin. (B) Rat oligodendrocytes and dorsal root ganglion (DRG) neurons were cocultured for 1–21 d in vitro (DIV), lysed, and used for immunoblotting with the respective antibodies for Rnd2, CNPase, MBP, and actin. (C) Oligodendrocytes were lysed and used for immunoblotting with the respective antibodies for Rnd2, CNPase, MBP, and actin. (D) Cross-sections of 7-, 14-, or 21-d-old mouse corpus callosum were costained with antibodies against Rnd2 (green) and PDGFRα, O4, or CC1 (red), respectively. Data are representative of multiple iterations. The scale bars indicate 50 μm. (E) The percentage of PDGFRα$^+$, O4$^+$, or CC1$^+$ cells among the Rnd2$^+$ cells is shown (n = 8–20 of total sections stained and counted from three sets of independent littermate mice). (F) Longitudinal sections of 14-d-old mouse corpus callosum were costained with antibodies against Rnd2 (green) and NF (red). Data are representative of multiple iterations. The scale bars indicate 50 μm.

of the g-ratios (Figure 5, G–I). At postnatal day 28, the average g-ratios were 0.787 ± 0.0890 in knockout mice compared with 0.822 ± 0.0876 in controls. Similar results were observed in 2-mo-old knockout mice (Figure 5J). The average g-ratios were 0.797 ± 0.0609 in knockout mice compared with 0.817 ± 0.0614 in controls (Figure 5, K–M), revealing that the increase in myelin thickness persists into adolescence.

On the basis of these findings, we set out to study whether Rnd2 is also involved in the regulation of later periods of oligodendrocyte myelination in vitro. We infected shRNAs for Rnd2 into oligodendrocytes and cocultured them with neurons for 28 d. Knockdown of Rnd2 in oligodendrocytes increased the amounts of MBP-positive cells and those of Olig2-positive cells expressing MBP at 28 d (Figure 6, A–C), whereas the amounts of NF proteins were comparable. The

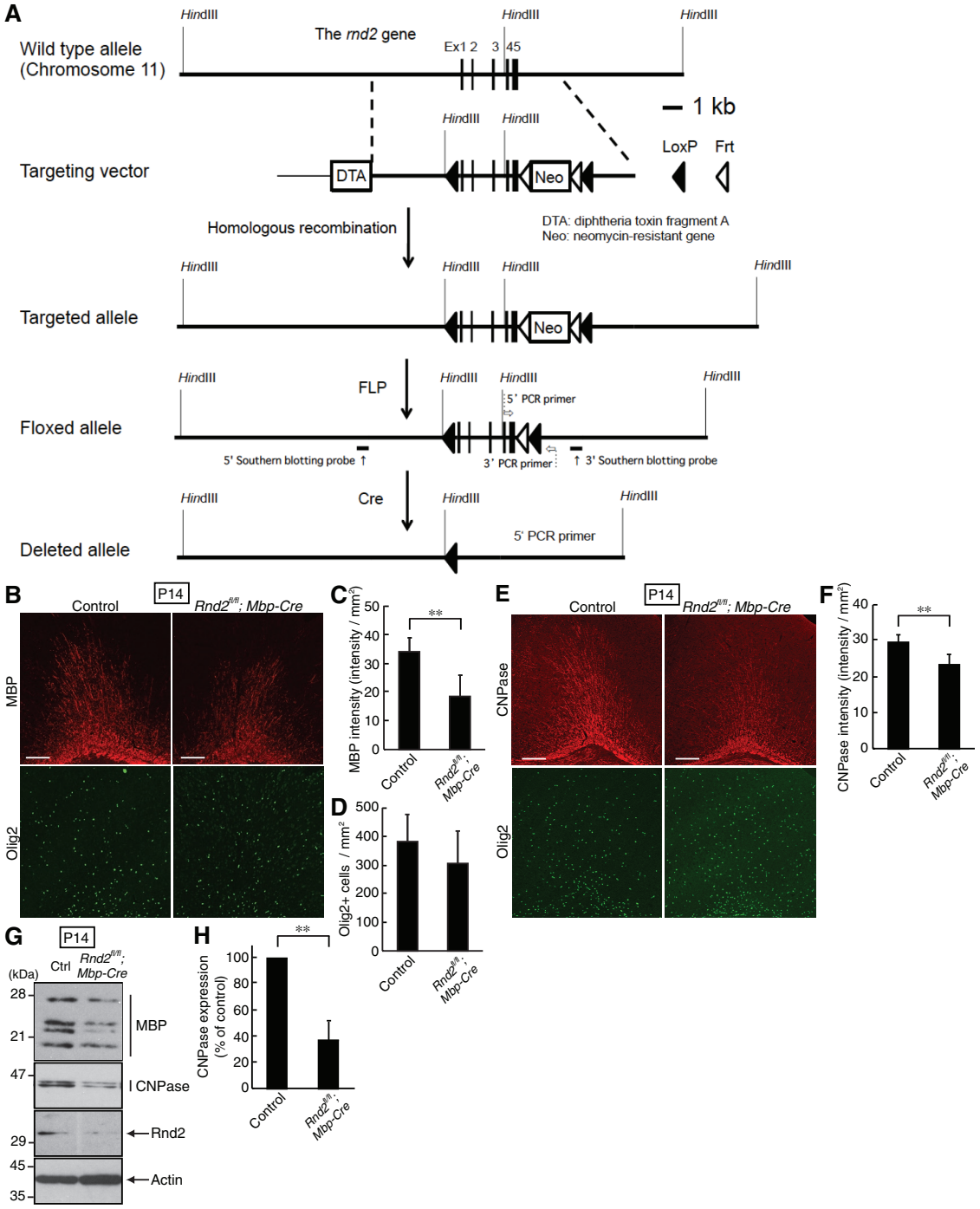

FIGURE 2: Mbp-Cre–mediated Rnd2 knockout mice exhibit decreased myelin marker protein expression at postnatal day 14. (A) Oligodendrocyte-specific MBP promoter–driven Cre recombinase transgenic mice were used for deletion of the loxP-flanked exons of the rnd2 gene. The knockout cassette as well as the primer and probe positions are shown. (B) Antibodies against MBP (red) and Olig2 (green) were used for costaining in 14-d-old Mbp-Cre–driven Rnd2 conditional knockout (*Rnd2*$^{fl/fl}$*; Mbp-Cre*) or control mouse brain cross-sections. The scale bars indicate 200 μm. (C) The intensity of MBP staining per square millimeter was relatively semiquantified (**, $p < 0.01$ in Student's *t* test; $n = 6$–8 of total sections stained and counted from three sets of independent littermate mice). (D) The Olig2$^+$ cells per square millimeter were counted ($n = 9$–12 of total sections stained and counted from three sets of independent littermate mice). (E) Brain cross-sections of conditional knockout (*Rnd2*$^{fl/fl}$*; Mbp-Cre*) and control mice at postnatal day 14 were costained with an anti-CNPase antibody (red) and Olig2 (green). The scale bars indicate 200 μm. (F) The intensity of CNPase staining per square millimeter was relatively semiquantified (**, $p < 0.01$ in Student's *t* test; $n = 6$ of total sections stained and counted from three sets of independent littermate mice). (G) Tissue lysates from 14-d-old conditional knockout or control (Ctrl) mouse whole brains were immunoblotted with an antibody against MBP, CNPase, Rnd2, or actin. (H) CNPase expression levels are shown statistically (**, $p < 0.01$ in Student's *t* test; $n = 4$ blots from four sets of independent littermate mice).

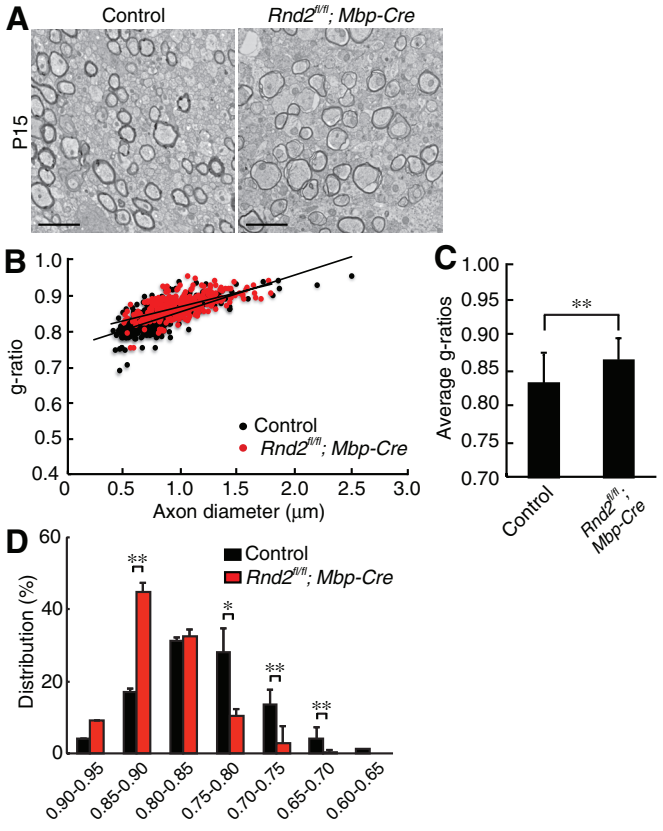

FIGURE 3: Mbp-Cre–mediated Rnd2 knockout mice exhibit decreased myelin thickness at postnatal day 15. (A) Electron microscopic images of the corpus callosum of conditional knockout (*Rnd2*$^{fl/fl}$*; Mbp-Cre*) and control mice at postnatal day 15 are shown. The scale bars indicate 2 μm. (B) Graph of g-ratios of myelinated axons for axon diameters is shown ($n = 343$ axons for three different knockout mice and $n = 297$ axons for their littermate controls). (C) Average g-ratios are shown (**, $p < 0.01$ in Student's *t* test). (D) Graph of the distributions of g-ratios is shown. (**, $p < 0.01$, *, $p < 0.05$ in one-way ANOVA).

total number of MBP-positive myelin segments and their lengths were increased (Figure 6, D and E). The number of Olig2-positive cells was comparable between control and Rnd2 knocked-down cocultures (Figure 6F). Consistent with these results from immunofluorescence studies, the expression levels of MBP and CNPase were increased by Rnd2 knockdown (Figure 6, G and H). Additionally, Rnd2 shRNAs were effective in cocultures even at 28 d (Figure 6G).

Together, these findings show that Rnd2 is involved in the inhibition of myelination in later periods of the myelination process.

Rnd2 Tg mice exhibit a phenotype opposite that of Rnd2 knockout mice

To confirm the knockout phenotype of Rnd2, we produced Rnd2 transgenic (Tg) mice. We injected a linearized transgene that contained the loxP-flanked multiple polyA sequences between the CAG promoter and the Rnd2 sequence into fertilized mouse eggs according to the standard method of generating Tg mice (Supplemental Figure S5, A–C) (Miyamoto *et al.*, 2014a). The Tg mice were crossbred with MBP promoter-controlled Cre recombinase Tg mice to generate Rnd2 conditional Tg mice (Supplemental Figure S5, A–C). In the resulting Rnd2; Mbp-Cre+/– Tg mouse line (one copy number of transgene, compared with positive control; tentatively referred to as a *Rnd2*^{Tg} mouse in the figure panels), the expression levels of Rnd2 in brains were markedly higher than those in controls (Figure 7A). The expression levels of the myelin marker proteins MBP and CNPase were markedly increased in 14-d-old Rnd2 Tg mice (Figure 7, A–C). Similarly, Rnd2 Tg mice exhibited increased CNPase staining levels compared with littermate controls (Figure 7, D and E). The number of cells positive for Olig2 was unchanged in Tg mice (Figure 7, D and F). Electron microscopic analysis of the corpus callosum revealed increased myelin thickness in 14-d-old Rnd2 Tg mice compared with control mice (Figure 7G). The average g-ratios in 14-d-old Rnd2 Tg mice were 0.830 ± 0.0446, whereas littermate controls had g-ratios of 0.857 ± 0.0376 (Figure 7, H–J).

On the other hand, Rnd2 Tg mice exhibited decreased expression levels of myelin marker proteins in brain tissues at postnatal day 28 (Figure 7, K–M). Myelin thickness in the corpus callosum was also decreased in Rnd2 Tg mice compared with controls (Figure 7, N and O; 0.864 ± 0.0500 in knockout mice and 0.811 ± 0.0786 in controls).

These results concerning the phenotypes in Tg mice support our findings in knockout mice.

Rnd2 regulates myelination signaling through Rho kinase

Rho and Rho kinase signaling regulates myelination by oligodendrocytes. Up-regulation of this signaling is associated with the inhibition of myelination, whereas down-regulation promotes it. As in the case of Rnd3 (Pacary *et al.*, 2011), Rnd2 inhibits the RhoA and Rho kinase signaling (Foster *et al.*, 1996). It has thus been likely that knockout of Rnd2 in mice up-regulates Rho kinase signaling and inhibits myelination at postnatal day 14. We performed immunoblotting of an active phosphorylated Rho kinase and a phosphorylated form of the Rho kinase substrate myosin-binding subunit (Mbs). At 14 d, the phosphorylation levels of Mbs and Rho kinase were increased in Rnd2 knockout mice, although the expression levels of their nonphosphorylated forms were comparable between control and knockout mice (Figure 8, A–C). At 28 d, on the other hand, the phosphorylation levels of Mbs and Rho kinase were decreased in Rnd2 knockout mice, while their expression levels remained comparable between the two genotypes (Figure 8, D–F). In keeping with these results, in Rnd2 Tg mice, the phosphorylation levels of Mbs and Rho kinase were decreased at 14 d, whereas they were increased at 28 d (Figure 8, G–L).

These findings show that, in early developmental periods, Rnd2 can inhibit Rho kinase signaling, possibly inhibiting myelination. In later periods, Rnd2 can promote Rho kinase signaling, possibly promoting myelination.

Rnd2 is involved in myelin maintenance in adulthood

Once we had discerned the role of Rnd2 in myelination during development, we next investigated whether Rnd2 is involved in myelin maintenance during adulthood. We crossbred Rnd2 floxed mice with tamoxifen (TAM)-inducible Plp1 promoter-controlled Cre recombinase transgenic mice (tentatively referred to as *Rnd2*$^{fl/fl}$*; Plp1-Cre*^{ERT} mice in the figure panels). Tamoxifen was administrated for 5 d to delete the *rnd2* gene in 8- to 9-wk-old Rnd2 knockout and control mice. Mouse tissues were harvested at different time points, and it was confirmed that, at 2 wk after tamoxifen administration, inducible knockout of Rnd2 decreased the intensities of MBP staining in the brain compared with control mice (Figure 9, A and B). The numbers of Olig2-positive cells were comparable between Rnd2 knockout and control mice (Figure 9, A and C). In addition, knockout of Rnd2 decreased the expression levels of MBP as well as those of CNPase (Figure 9, D and E).

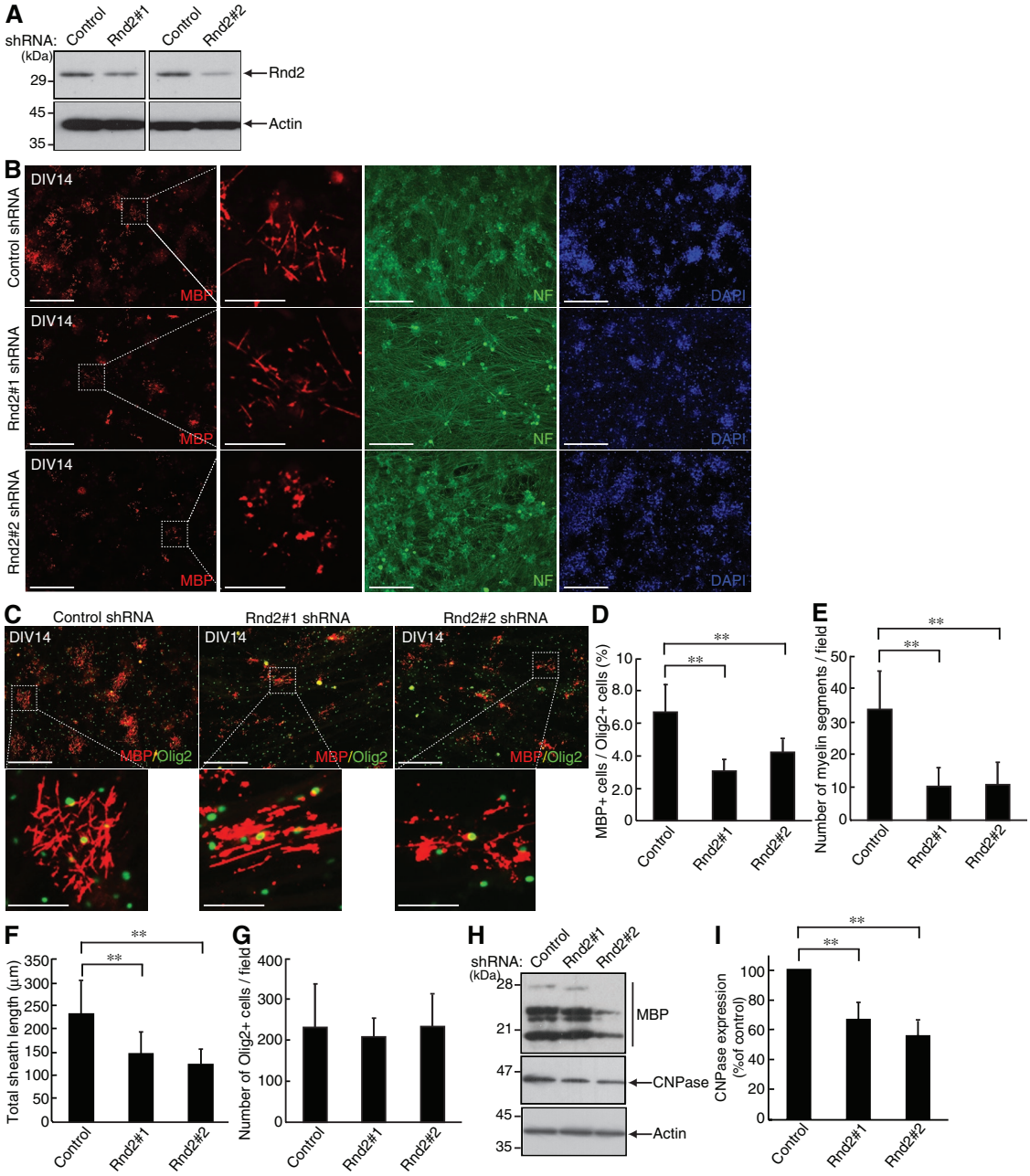

FIGURE 4: Knockdown of Rnd2 decreases myelin formation in cocultures at 21 d. (A) Knockdown efficiencies of two nonoverlapping shRNAs (Rnd2#1 and Rnd2#2) were confirmed by immunoblotting. (B) Oligodendrocytes that had been transfected with Rnd2 shRNAs or control cells were cocultured with neurons for 21 d and then costained with antibodies against MBP (red), NF (green), and DAPI (blue) in order to detect myelin segments in regions of interest. The scale bars indicate 200 μm. Magnified views of the myelinated oligodendrocytes in the dotted white squares are also shown. The scale bars indicate 50 μm. (C) Oligodendrocytes that had been transfected with Rnd2 shRNAs or control cells were cocultured with neurons for 21 d and then costained with antibodies against MBP (red) and Olig2 (green). The scale bars indicate 200 μm. Magnified views of the myelinated oligodendrocytes in the dotted white squares are also shown. The scale bars indicate 50 μm. (D) The percentage of MBP^+ cells among the $Olig2^+$ cells per field (**, $p < 0.01$ in one-way ANOVA; $n = 8$–12 fields of three independent experiments). (E) The myelin segments per field were counted (**, $p < 0.01$ in one-way ANOVA; $n = 10$–11 fields of three independent experiments). (F) The total sheath length of myelinated oligodendrocytes per field was measured (**, $p < 0.01$ in one-way ANOVA; $n = 15$ fields of three independent experiments). (G) The number of $Olig2^+$ cells per field is shown ($n = 8$–12 fields of three independent experiments). (H) The lysates were immunoblotted with an antibody against MBP, CNPase, or actin. (I) CNPase expression levels are shown statistically (**, $p < 0.01$ in Student's t test; $n = 4$ blots of four independent experiments).

Next, we analyzed the myelin sheath ultrastructure by electron microscopy. We observed that Rnd2 knockout mice exhibited decreased myelin thickness in the corpus callosum (Figure 9F). The average g-ratios were 0.817 ± 0.0595 in Rnd2 knockout mice and 0.807 ± 0.0612 in controls (Figure 9, G–I). Together, these findings suggest that Rnd2 can positively regulate short-term myelin maintenance in adulthood.

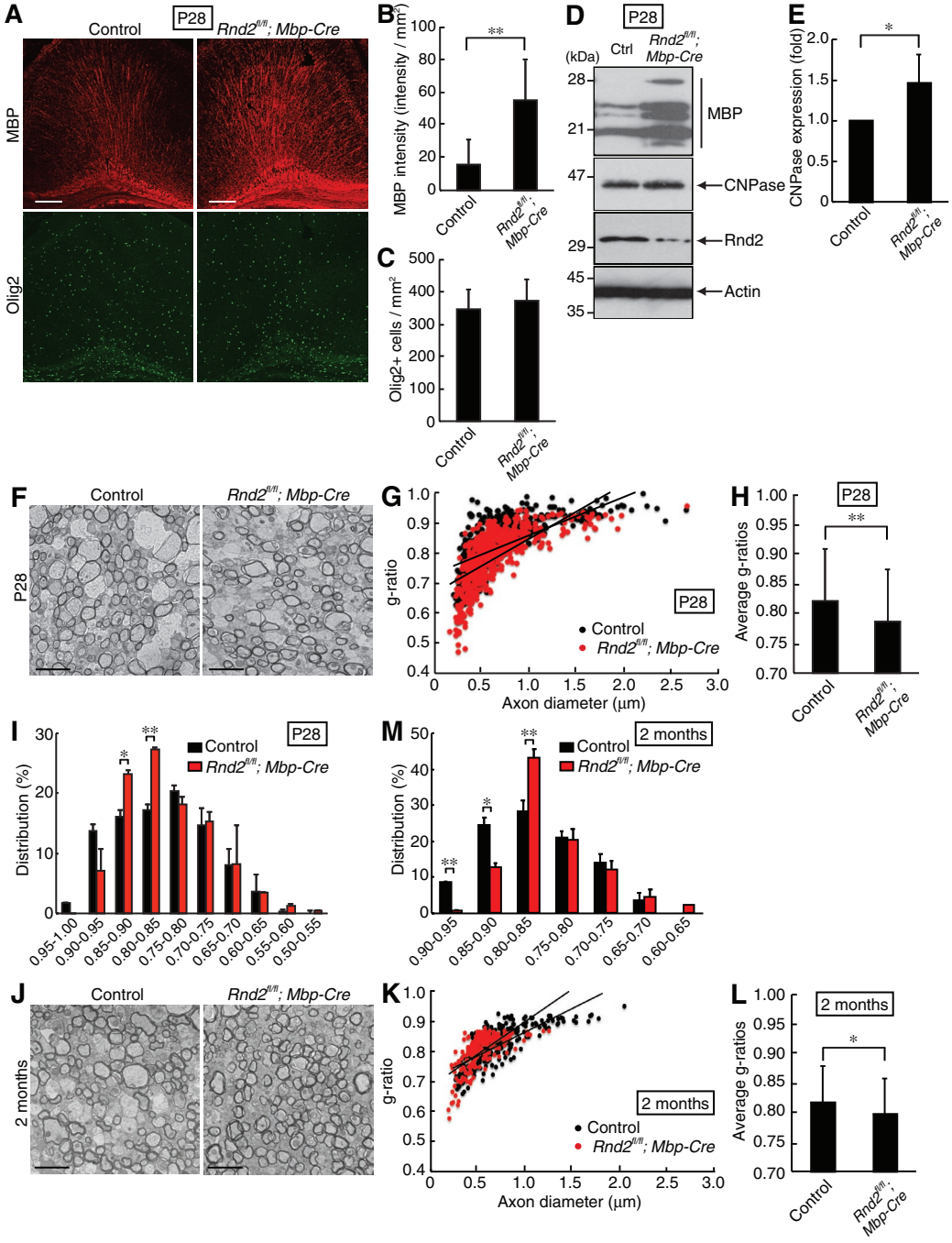

FIGURE 5: Mbp-Cre–mediated Rnd2 knockout mice exhibit increased myelin marker protein expression and myelin thickness at postnatal day 28. (A) Brain coronal sections of conditional knockout (*Rnd2*$^{fl/fl}$*; Mbp-Cre*) and control mice at postnatal day 28 were costained with an anti-MBP antibody (red) and Olig2 (green). The scale bars indicate 200 μm. (B) The intensity of MBP staining per square millimeter was relatively semiquantified (**, $p < 0.01$ in Student's *t* test; $n = 10$ of total sections stained and counted from three sets of independent littermate mice). (C) The Olig2$^+$ cells per square millimeter were counted ($n = 6$–10 of total sections stained and counted from three sets of independent littermate mice). (D) Tissue lysates from 28-d-old brains were immunoblotted with an antibody against MBP, CNPase, Rnd2, or actin. (E) CNPase expression levels are shown statistically (*, $p < 0.05$ in Student's *t* test; $n = 4$ blots from four sets of independent littermate mice). (F) Electron microscopic images of the corpus callosum of conditional knockout (*Rnd2*$^{fl/fl}$*; Mbp-Cre*) and control mice at postnatal day 28 are shown. The scale bars indicate 2 μm. (G) Graph of g-ratios of myelinated axons for axon diameters is shown ($n = 514$ axons for three different knockout mice and $n = 504$ axons for their littermate controls). (H) Average g-ratios are shown (**, $p < 0.01$ in Student's *t* test). (I) Graph of the distributions of g-ratios is shown (**, $p < 0.01$, *, $p < 0.05$ in one-way ANOVA). (J) Electron microscopic images of the corpus callosum of conditional knockout and control mice at 2 mo are shown. The scale bars indicate 2 μm. (K) Graph of the g-ratios of myelinated axons for axon diameters is shown ($n = 297$ axons for three different knockout mice and $n = 287$ axons for their littermate controls). (L) Average g-ratios are shown (**, $p < 0.01$ in Student's *t* test). (M) Graph of the distributions of g-ratios is shown (**, $p < 0.01$, *, $p < 0.05$ in one-way ANOVA).

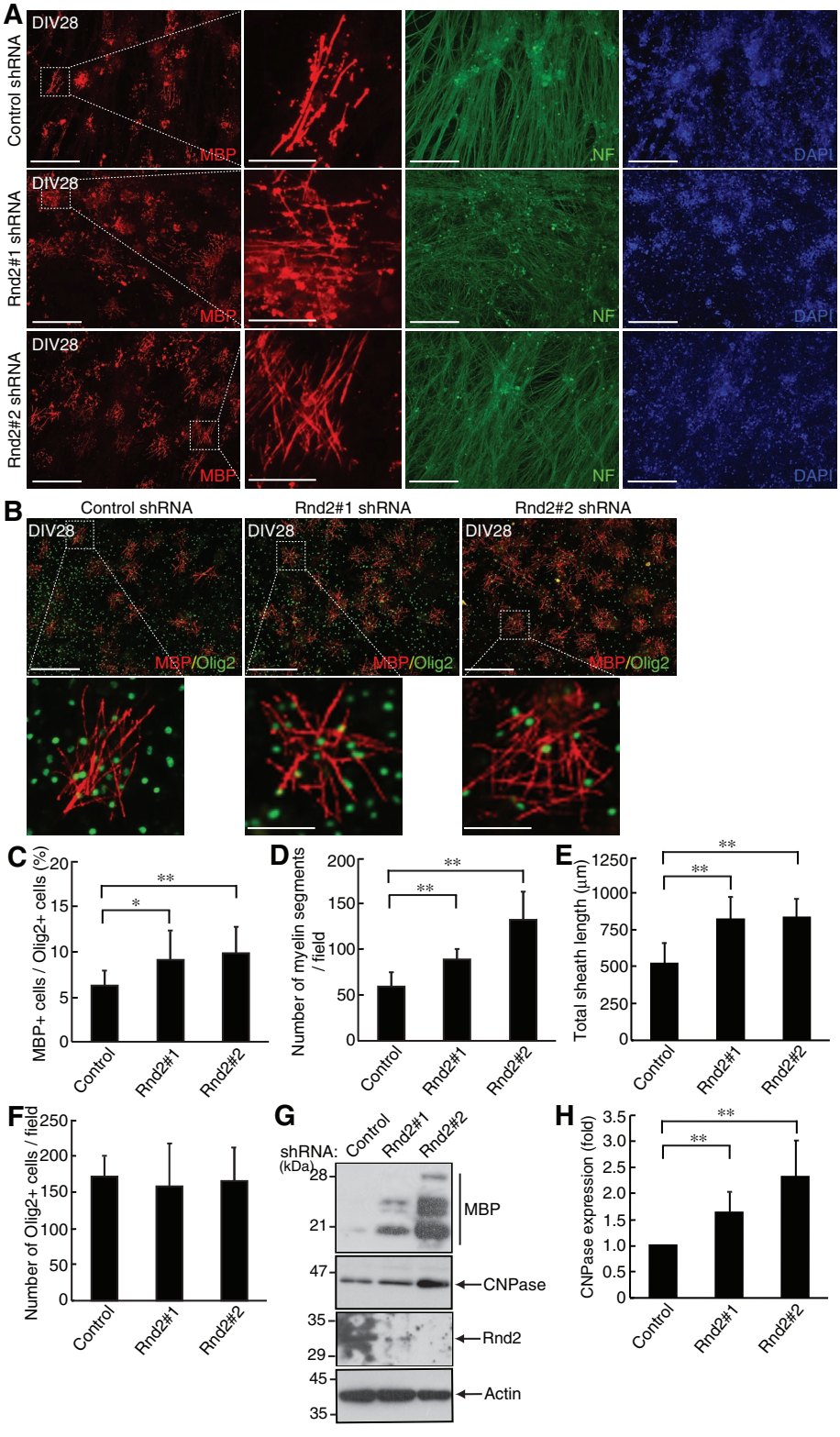

FIGURE 6: Knockdown of Rnd2 increases myelin formation in cocultures at 28 d. (A) Oligodendrocytes that had been transfected with Rnd2 shRNAs or control cells were cocultured with neurons for 28 d and then costained with antibodies against MBP (red), NF (green), and DAPI (blue). The scale bars indicate 200 μm. Magnified views of the myelinated oligodendrocytes in the dotted white squares are also shown. The scale bars indicate 50 μm. (B) Oligodendrocytes that had been transfected with Rnd2 shRNAs or control cells were cocultured with neurons for 28 d and then costained with antibodies against MBP (red) and Olig2 (green). The scale bars indicate 200 μm. Magnified views of the myelinated oligodendrocytes in the dotted white squares are also shown. The scale bars indicate 50 μm. (C) The percentage of MBP$^+$ cells among the Olig2$^+$ cells per field (**, $p < 0.01$, *, $p < 0.05$ in one-way ANOVA; $n = 6$–7 fields of three independent experiments). (D) The myelin segments per field were counted (**, $p < 0.01$ in one-way ANOVA; $n = 17$–25 fields of three independent experiments). (E) The total sheath length of myelinated oligodendrocytes per field was measured (**, $p < 0.01$ in one-way ANOVA; $n = 22$ fields of three independent experiments). (F) The number of Olig2$^+$ cells per field is shown ($n = 6$–9 fields of three independent experiments). (G) The lysates were immunoblotted with an antibody against MBP, CNPase, Rnd2, or actin. (H) CNPase expression levels are shown statistically (**, $p < 0.01$ in Student's t test; $n = 5$ blots from four independent experiments).

To further investigate the effect of Rnd2 knockout in myelin maintenance, we performed MBP staining at 4 wk after tamoxifen administration. Knockout of Rnd2 increased MBP intensity in the brain (Figure 10, A and B), whereas the number of Olig2-positive cells was unchanged (Figure 10, A and C). Immunoblotting revealed that the expression levels of MBP and CNPase were greater in Rnd2 knockout mice that in control mice (Figure 10, D and E).

We analyzed the myelin sheath ultrastructure and observed that inducible knockout mice exhibited increased myelin thickness in the corpus callosum compared with controls (Figure 10F). The average g-ratios were 0.775 ± 0.0854 in knockout mice and 0.807 ± 0.0701 in controls (Figure 10, G–I).

Collectively, these results suggest that the effects of Rnd2 on myelination during development persist during myelin maintenance.

DISCUSSION

Oligodendrocyte myelination requires dramatic growth of the plasma membranes such that they form multiple layers around axons. Surprisingly, the collective areas of these differentiated plasma membranes often increase to more than one hundred times the areas of the plasma membranes of the oligodendrocytes before myelination. Myelination requires continuous and dynamic oligodendrocyte morphogenesis, in which a variety of intracellular as well as extracellular signaling molecules are involved in controlling cell morphological changes (Bradl and Lassmann, 2010; Simons and Lyons, 2013; Bergles and Richardson, 2015; Saab and Nave, 2017). It has been proposed that the switching of mechanisms on and off by their signaling molecules is required to

achieve the precise morphological changes that are necessary (Bradl and Lassmann, 2010; Simons and Lyons, 2013; Bergles and Richardson, 2015; Saab and Nave, 2017).

Among the small GTPase family proteins controlling the intracellular molecules that switch these mechanisms on and off, increasing evidence indicates that, in addition to the Rho GTPases, including Rnd2, the Ras GTPases also play important roles in oligodendrocyte myelination, acting through the activation of many signal transduction pathways (Bennett *et al.*, 2003). Interestingly, the downstream signaling of Rho GTPases is quite similar to that of Ras GTPases (Devreotes and Horwitz, 2015). For example, in addition to the prototypic Ras proteins such as H-, K-, and N-Ras, R-Ras1/2 have been reported to be critical for oligodendrocyte differentiation and myelination (Sanz-Rodriguez *et al.*, 2018). R-Ras1/2 are expressed in oligodendrocytes at almost equal levels. Mice knocking out both R-Ras1/2 exhibit decreased myelin thickness in the optic nerves. The phenotypes seen in double-knockout mice are presumed to be due to the down-regulation of phosphatidylinositol-3 kinase (PI3K) forming 3-phosphoinositides (Sanz-Rodriguez *et al.*, 2018). Signaling through PI3K stimulates a molecular pathway that is indispensable for myelination and that includes the unique Ras family members Rheb1/2 as well as their regulators such as the tuberous sclerosis complex 1/2 (TSC1/2). Rheb1/2 are involved in the regulation of cell spreading and cell volumes in oligodendrocytes as well as their energy metabolisms. Indeed, deleting Rheb1 in mice results in delayed oligodendrocyte differentiation and decreased myelin formation (Zou *et al.*, 2014). Additionally, the final amounts of 3-phosphoinositides in cells are based on the degree of balance between their phosphorylation and dephosphorylation. Sufficient balance between the activities of PI3K and those of the phosphatases dephosphorylating 3-phosphoinositides is needed to properly trigger myelination. Actually, conditional knockout of phosphatase and the tensin homologue deleted from chromosome 10 (PTEN) in mice typically results in enhanced myelin thickness leading to excessive myelin membrane formation (Goebbels *et al.*, 2010). The presence of regulatory networks underlying Ras and Rho GTPases as well as the related on-and-off signaling mechanisms that operate in myelination during development reminds us of the presence of other small GTPase networks, which have turned out to be more complicated than earlier studies on myelination had indicated (Thurnherr *et al.*, 2006). It is conceivable that molecules belonging to identified or unidentified networks positively and negatively control continuous and dynamic myelination at different developmental periods as needed.

This study is the first to show that Rnd2, a unique Rnd subfamily molecule belonging to the Rho family of small GTPases, acts as one of the regulators of oligodendrocyte myelination in mice. Our findings reveal that Rnd2 has different effects on myelination at different developmental periods. In earlier developmental stages, that is, shortly after birth, oligodendrocyte-specific knockout of Rnd2 has a negative effect on myelin sheath formation without affecting the number of oligodendrocyte lineage cells. The effect of Rnd2 on myelination could in part be explained by the activities of Rho kinase, which is the negative regulator of myelination (Zhao *et al.*, 2007), given that Rnd2 knockout increased the amounts of active phosphorylated forms of Rho kinase. Oligodendrocyte-specific transgenic mice of Rnd2, on the other hand, exhibited enhanced myelin thickness. As we now know, Rnd2 plays a role in inhibiting myelination in later periods, possibly by breaking down excessively thick myelin membranes, as suggested by the fact that Rnd2 knockout and transgenic mice exhibit increased and decreased myelin thickness, respectively. Rnd2 knockout also decreases the phosphorylation levels of Rho kinase (these results are summarized in Table 2 and Figure 11). The variable effects of Rnd2 on myelination depending on developmental period have also been noted in studies knocking out Rnd2 specifically in adult mice. The phenomenon whereby Rnd2 regulates myelination differently in different periods is likely to be reflected in Rnd2's effects on myelin maintenance in adult mice. It may be of interest that Rnd2 has two roles in myelination during development, one as a negative regulator and one as a positive regulator.

It remains unclear how Rnd2 affects Rho kinase and other possible signaling molecules differentially to regulate myelination. It may be because Rnd2 affects Rho kinase by the on-and-off switching mechanism of RhoA through different effectors at different periods. It is well known that p190RhoGAP A/B, which inactivate RhoA, are the effectors of the Rnd2 homologues Rnd1/3, whose interaction results in antagonizes the activities of RhoA, and in turn, Rho kinase (Wennerberg *et al.*, 2003). Because Rnd2 seems to bind directly to p190RhoGAP proteins in silico (URL: https://thebiogrid.org/), it is possible that Rnd2 inactivates RhoA and Rho kinase through p190RhoGAP proteins, leading to a positive effect on myelination in earlier developmental periods. Additionally, Rnd2 can indirectly activate RhoA through the Rnd2 effector Pragmin (also called pseudopodium-enriched atypical kinase 1-related, kinase-activating pseudokinase 1 [PRAG1], Tanaka *et al.*, 2006). Rnd2's interaction with Pragmin may have a negative regulatory effect on myelination in later developmental periods; although the expression levels of Rnd2 increase continuously during development, those of Pragmin in the brain remain steady and are not up-regulated from the embryonic stage to adulthood (Tanaka *et al.*, 2006). It is reasonable to presume that one of the molecular mechanisms underlying the differential effects of Rnd2 on myelination is related to differences in the levels of identified or unidentified Rnd2 effector proteins at different developmental periods.

Further studies will promote our understanding not only of the detailed mechanisms by which Rnd2 is differentially involved in the regulation of oligodendrocyte myelination at different developmental periods but also of how Rnd2 regulates myelin maintenance. Such studies will yield information that may elucidate positive and negative regulatory mechanisms triggering oligodendrocyte myelination.

MATERIALS AND METHODS

Request a protocol through *Bio-protocol*.

Antibodies

The following antibodies were purchased: rabbit polyclonal anti-Rnd2 from Proteintech (Rosemont, IL); mouse monoclonal anti-myelin basic protein (MBP), and rabbit polyclonal anti-glial fibrillary acidic protein (GFAP) from Covance (Princeton, NJ); mouse monoclonal anti–β-actin from Fujifilm (Tokyo, Japan); goat polyclonal anti–platelet-derived growth factor receptor (PDGFR) α from Santa Cruz Biotechnology (Santa Cruz, CA); mouse monoclonal anti-MBP, mouse monoclonal anti–adenomatus polyposis coli (APC) (also called CC1), mouse monoclonal anti-O4, and mouse monoclonal anti-NeuN from Merck-Millipore (Billerica, MA); rabbit polyclonal anti–phosphorylated Thr696-Mbs and rabbit polyclonal anti-Mbs from Cell Signaling Technology (Danvers, MA); rabbit monoclonal anti-Olig2, rabbit polyclonal anti–phosphorylated Ser1366-Rho kinase, which recognizes active states, and rabbit polyclonal anti-Rho kinase from Abcam (Cambridge, UK); mouse monoclonal anti-2′, 3′-cyclicnucleotide 3′-phosphodiesterase (CNPase) and rabbit polyclonal anti-neurofilament (NF) large subunit from Sigma-Aldrich

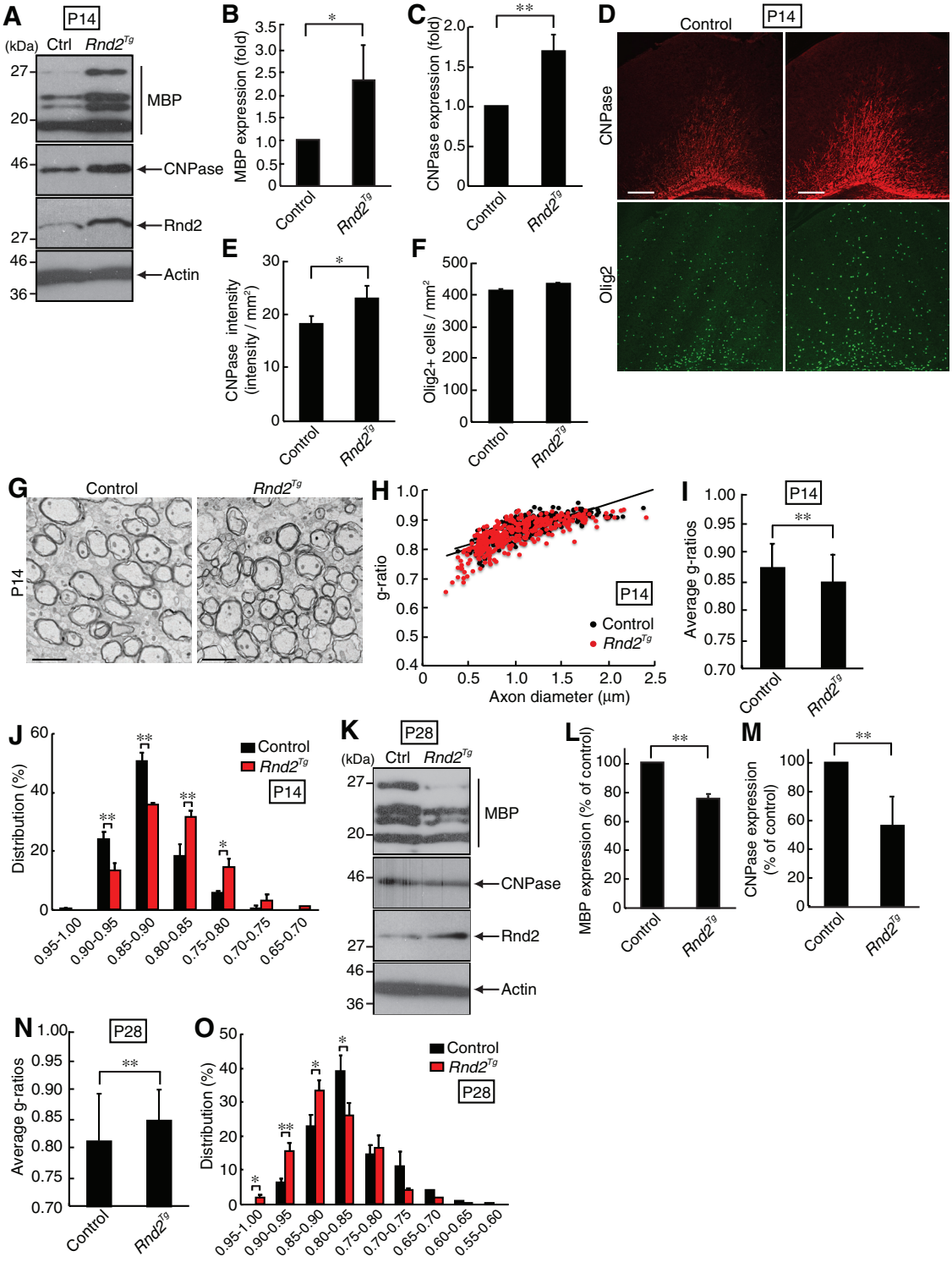

FIGURE 7: Rnd2 transgenic mice exhibit increased myelin marker protein expression and myelin thickness at postnatal day 14, whereas both are decreased in transgenic mice at postnatal day 28. (A) Tissue lysates from 14-d-old Rnd2 transgenic (*Rnd2*^{Tg}) and control mouse brains were immunoblotted with an antibody against MBP, CNPase, Rnd2, or actin. (B) MBP expression levels are shown statistically (*, $p < 0.05$ in Student's *t* test; $n = 4$ blots from four different sets of littermate mice) (C) CNPase expression levels are shown statistically (**, $p < 0.01$ in Student's *t* test; $n = 5$ blots from five different sets of littermates). (D) Brain cross-sections of Rnd2 transgenic (*Rnd2*^{Tg}) and control mice at postnatal day 14 were costained with an anti-CNPase antibody (red) and Olig2 (green). The scale bars indicate 200 μm. (E) The intensity of CNPase staining per square millimeter was relatively semiquantified (*, $p < 0.05$ in Student's *t* test; $n = 5$ sections from three different sets of littermates). (F) The Olig2$^+$ cells per square millimeter were counted ($n = 9$–12 sections from three different sets of littermates). (G) Electron microscopic data of 14-d-old corpus callosum are shown. The scale bars indicate 2 μm. (H) Graph of g-ratios of myelinated axons for axon diameters is shown ($n = 289$ axons for

(St. Louis, MO); peroxidase-conjugated secondary antibodies from MBL (Nagoya, Japan); and fluorescence-labeled secondary antibodies from Thermo Fisher Scientific (Waltham, MA).

Generation of Rnd2 conditional knockout mice

A genomic region containing exons 1–5 of *rnd2* was obtained from a C57BL/6 mouse genomic library (Unitech, Chiba, Japan). The targeting vector was constructed to replace the original exons 1–5 with the diphtheria toxin, loxP, the exons 1–5, and Frt-flanked neomycin-resistant sequences. C57BL/6 embryonic stem (ES) cells were transfected with the linearized targeting vector by electroporation. G418-resistant, homologous recombination, positive transfectants were isolated, and their genomic sequences were confirmed. These ES cells were used for generating chimeric mice.

First, to identify the neo gene containing the Rnd2 knockout cassette, offspring were genotyped by genomic PCR. To evaluate the knockout cassette allele, the primers used were 5′-GCCGGCGCGTAGCCGGGACC-3′ (sense) and 5′-CGAACACCTGCAGCAACGCTGTCTTG-3′ (antisense) for the knockout cassette long-arm position and 5′-CGTGCAATCCATCTTGTTCAAT-3′ (sense) and 5′-TGAACCTGCTTTGTATCAGAAGTGC-3′ (antisense) for the knockout cassette short-arm position. In the former primer pair, the allele-harboring knockout cassette displayed ~160 base pairs. In the later primer pair, the allele-harboring knockout cassette displayed ~3500 base pairs, enabling us to obtain 11 chimeric mice.

Next, to remove the neo gene, offspring were mated with Unitech Flp recombinase transgenic mice (Unitech). To evaluate the neo gene deletion allele, the primers used were 5′-AAGTGGGAGCTGTGTCCTACGTT-3′ (sense) and 5′-GAGGTCAAAAAGTCCAGGACGAC-3′ (antisense) for the long-arm position and 5′-GAACAAGATGGATTGCACGCAGGTTCTCCG-3′ (sense) and 5′-GTAGCCAACGCTATGTCCTGATAG-3′ (antisense) for the neo gene. In the former primer pair, the knockout allele with the neo gene, the knockout allele without the neo gene (also called the floxed allele), and the wild-type allele displayed ~2020, ~470, and ~310 base pairs, respectively. In the later primer pair, the knockout allele with the neo gene displayed ~670 base pairs, enabling us to obtain a single kind of ES cell–derived 7 hemizygotic floxed knockout mice.

Finally, to remove the flp gene, these mice were further mated with wild-type C57BL/6 mice. The primers used were 5′-TAGTTTGCAATTACAGTTCGAATCA-3′ (sense) and 5′-AGCCTTGTTGTACGATCTGACTAAG-3′ (antisense) for the flp gene, whose removed allele displayed ~500 base pairs.

The primers used for Rnd2 conditional knockout mouse genotyping were 5′-AAGTGGGAGCTGTGTCCTACGTT-3′ (sense) and 5′-GAGGTCAAAAAGTCCAGGACGAC-3′ (antisense). The floxed and the wild-type alleles displayed ~470 and ~310 base pairs, respectively. Southern blotting, using the 5′ or 3′ region of exons of the gene encoding Rnd2 as the specific probe, confirmed that the floxed and wild-type alleles were ~7.5 and ~9.8 kbp for the 5′ probe or ~7.6 and ~3.7 kbp for the 3′ probe, respectively.

To delete the gene specifically in oligodendrocytes, Rnd2 conditional knockout mice were mated with MBP promoter– Cre recombinase transgenic mice (RBRC No. 01461; Riken BioResource Center, Ibaraki, Japan) or tamoxifen-inducible PLP1 promoter–driven Cre recombinase transgenic mice (JAX No. 005975; The Jackson Laboratory, Bar Harbor, ME). These transgenic mice were mated with wild-type C57BL/6 mice for more than 12 generations to achieve the same background as the other genetically modified mice. Genomic PCRs were performed according to established standard protocols (Riken BioResource Center or The Jackson Laboratory). The primer pair for Cre recombinase transgenic mice was 5′-CCACCACCTCTCCATTGCAC-3′ (sense) and 5′-ATGTTTAGCTGGCCCAAATG-3′ (antisense), displaying ~500 base pairs.

To show that Cre was active in MBP-expressing tissues, we performed PCR amplification using the mouse corpus callosum genome. The primer pair was 5′-CTTTCCACTCAGTACTTGGCTAGAG-3′ (sense) and 5′-AGAGAAGGGATAAGGGTGTAGAGAA-3′ (antisense). The floxed and deleted alleles displayed ~3.9 and ~1.0 kbp, respectively.

Mouse tail genetic PCR amplification (KAPA mouse genotyping kit; NIPPON Genetics Co., Ltd., Tokyo, Japan) was routinely performed in 35 cycles, with each cycle consisting of denaturation at 94°C for 10 or 15 s, annealing at 58 to 68°C (depending on each primer's T_m value) for 15 s, and extension at 68 to 72°C for 15 or 30 s (depending on product length).

When it was possible to determine their sex, male mice were used for experiments. All homozygous mice, as well as their heterozygous mice, were fertile under standard breeding conditions.

Generation of Rnd2 conditional transgenic mice

An ~4.5 kbp DNA fragment containing the CAG promoter, loxP, triple SV40 polyAs, loxP, human Rnd2, and single SV40 polyA sequences (Vector Builder, Chicago, IL) was digested from the backbone vector VB180809 with *Apa*LI restriction enzyme and injected into fertilized BDF1 oocytes (Miyamoto *et al*., 2014a). Transgenic founder mice and established transgenic mice were identified by both genomic PCR (840 base pairs of length) using tail DNA with the specific primer pair (5′-CAGGTGTTCGCCAAGGACGCCTATC-3′ [sense] and 5′-CCTCCCACACCTCCCCCTGAAC-3′ [antisense] for Rnd2) and by Southern blotting with *Eco*RI-digested tail DNA hybridized to a radioisotope-labeled probe for the internal Rnd2 sequence of the transgene (~700 base pairs of hybridized band). Genomic PCR was performed in 35 cycles, each consisting of denaturation at 94°C for 15 s, annealing at 63°C for 15 s, and extension at 72°C for 15 s. We succeeded in generating five founder mice, each harboring one or more transgenes, which were mated to wild-type C57BL/6J mice. The transgenes in two transgenic lines were stably maintained for at least three generations. Among them, one line was used in the following experiments. The transgenic mice were fertile and engaged in normal behavior under standard breeding conditions. Male mice were used for experiments when their gender was distinguishable.

three different transgenic mice and $n = 273$ axons for their littermate controls). (I) Average g-ratios are shown (**, $p < 0.01$ in Student's *t* test). (J) Graph of the distributions of g-ratios is shown (**, $p < 0.01$, *, $p < 0.05$ in one-way ANOVA). (K) Tissue lysates from 28-d-old Rnd2 transgenic and control (Ctrl) mouse brains were immunoblotted with an antibody against MBP, CNPase, Rnd2, or actin. (L) MBP expression levels at 28 d are shown statistically (**, $p < 0.01$ in Student's *t* test; $n = 3$ blots from three different sets of littermates). (M) CNPase expression levels at 28 d are shown statistically (**, $p < 0.01$ in Student's *t* test; $n = 3$ blots from three different sets of littermates). (N) Average g-ratios ($n = 309$ axons for three different transgenic mice and $n = 291$ axons for their littermate controls) at 28 d are shown (**, $p < 0.01$ in Student's *t* test). (O) Graph of the distributions of g-ratios is shown (**, $p < 0.01$, *, $p < 0.05$ in one-way ANOVA).

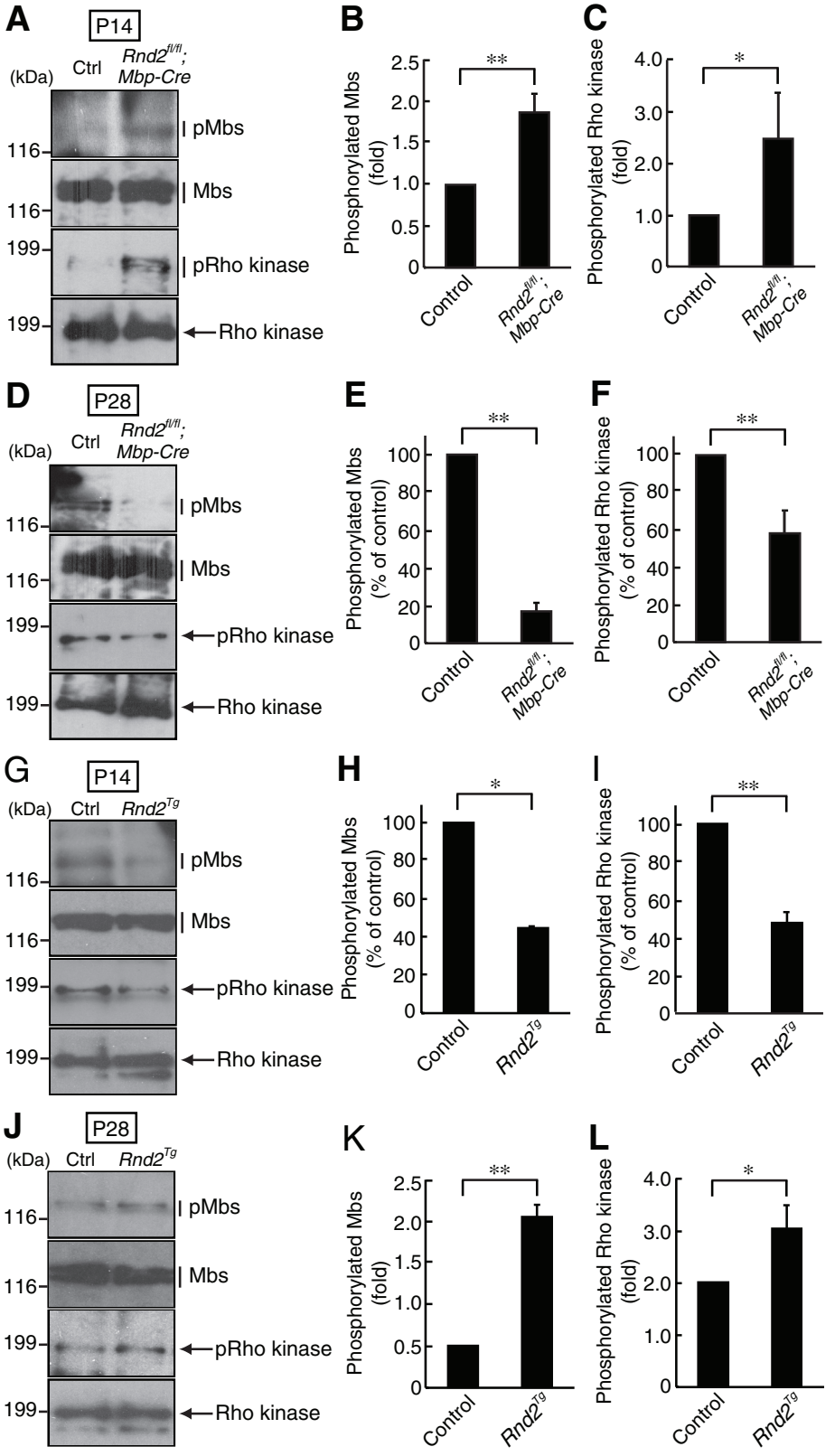

FIGURE 8: Mbp-Cre–mediated Rnd2 knockout mice exhibit increased Rho kinase signaling at postnatal day 14 and decreased Rho kinase signaling at postnatal day 28. (A) Tissue lysates from 14-d-old conditional knockout (*Rnd2*$^{fl/fl}$*; Mbp-Cre*) and control mice were used for immunoblotting with the respective antibodies for phosphorylated Mbs (pMbs), Mbs, phosphorylated Rho kinase (pRho kinase), and Rho kinase are shown. (B, C) Statistical data of phosphorylated Mbs and phosphorylated Rho kinase (**, $p < 0.01$, *, $p < 0.05$ in Student's *t* test; $n = 4$ blots from four different sets of littermates). (D) Tissue lysates from 28-d-old conditional knockout (*Rnd2*$^{fl/fl}$*; Mbp-Cre*) and control mice were used for immunoblotting with the respective antibodies for pMbs, Mbs, pRho kinase, and Rho kinase and are shown. (E, F) Statistical data of phosphorylated Mbs and phosphorylated Rho kinase. (**, $p < 0.01$ in Student's *t* test; $n = 6$ blots from six different sets of littermates). (G) Tissue lysates from 14-d-old Rnd2 transgenic (*Rnd2*^{Tg}) and control mice were used for immunoblotting with the respective antibodies for pMbs, Mbs, pRho kinase, and Rho kinase. (H, I) Statistical data of phosphorylated Mbs and phosphorylated Rho kinase are shown (**, $p < 0.01$, *, $p < 0.05$ in Student's *t* test; $n = 3$ blots from three different sets of littermates). (J) Tissue lysates from 28-d-old Rnd2 transgenic and control mice were used for immunoblotting with the respective antibodies for pMbs, Mbs, pRho kinase, and Rho kinase. (K, L) Statistical data of phosphorylated Mbs and phosphorylated Rho kinase are shown. (**, $p < 0.01$ in Student's *t* test; $n = 3$ blots from three different sets of littermates).

To induce the gene specifically in oligodendrocytes, Rnd2 conditional transgenic mice were mated with MBP promoter–driven Cre recombinase transgenic mice. The primer pair for genomic PCR was 5′-CCACCACCTCTCCATTGCAC-3′ (sense) and 5′-ATGTTTAGCTGGCCCAAATG-3′ (antisense), displaying ~500 base pairs (The Jackson Laboratory).

Tamoxifen treatment in vivo

Tamoxifen (TAM; Sigma-Aldrich) was dissolved in a mixture of 90% corn oil and 10% ethanol at a concentration of 10 mg/ml. Eight- to nine-week-old mice were given a daily intraperitoneal injection of 1 mg (100 µl) TAM for 5 consecutive days (Miyamoto *et al.*, 2016). The first day of injections was designated as day 0.

Preparation of plasmids containing short-hairpin RNAs

All nucleotide sequences were confirmed by sequencing. The sense and antisense oligonucleotides, which were used for duplex production, were as follows. Rnd2#1 (starting from nucleotide 339 of rat Rnd2) shRNA is composed of 5′-GATCCGGTGGTGTTGGTTGGTTGTCTGTGAAGCCACAGATGGGACAGCCAACCAGCACCACCTTTTTTACGCGTAT-3′ (sense) and 5′-CGATACGCGTAAAAAAGGTGGTGCTGGTTGGCTGTCCCATCTGTGGCTTCACAGACAACCAACCAACACCACCG-3′ (antisense); Rnd2#2 (starting from nucleotide 405 of rat Rnd2) shRNA is

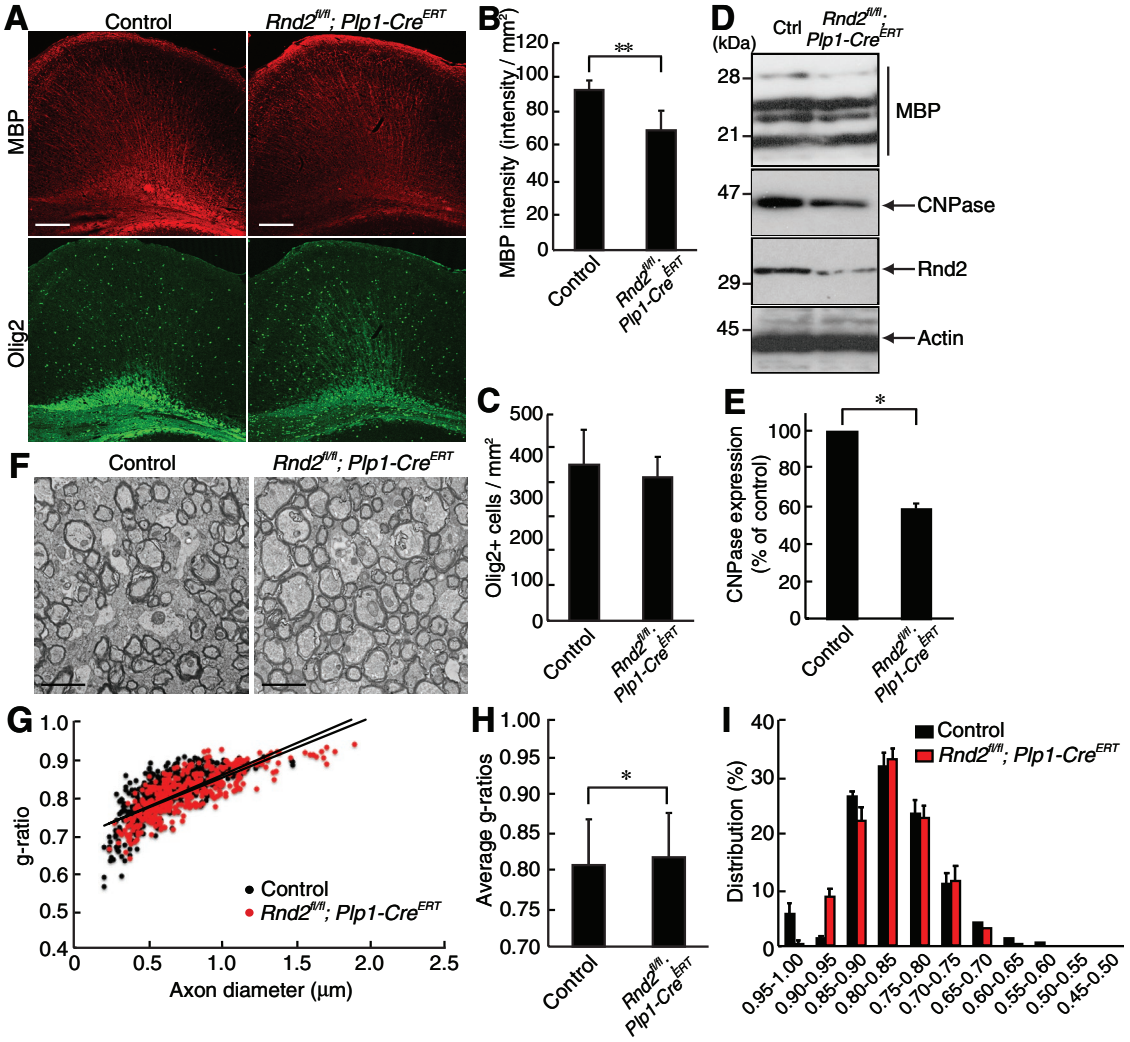

FIGURE 9: Plp1-Cre^{ERT}–mediated Rnd2 knockout mice exhibit decreased myelin thickness in adult mice at 2 wk after tamoxifen administration. (A) Eight- or nine-week-old mice were given a daily injection of 1 mg (100 µl) tamoxifen (TAM) for 5 consecutive days. Two weeks following the final TAM injection, antibodies against MBP (red) and Olig2 (green) were used for costaining in TAM-treated *Rnd2*$^{fl/fl}$*; Plp1-Cre*^{ERT}or control mouse brain cross-sections. The scale bars indicate 200 µm. (B) The intensity of MBP staining per square millimeter was relatively semiquantified (**, $p < 0.01$ in Student's *t* test; $n = 6$–7 sections from three different sets of littermates). (C) The Olig2$^+$ cells per square millimeter were counted ($n = 7$ sections from three different sets of littermates). (D) The brain lysates from TAM-treated Plp1-Cre^{ERT}–driven Rnd2 conditional knockout or control mice were immunoblotted with an antibody against MBP, CNPase, Rnd2, or actin. (E) CNPase expression levels are shown statistically (*, $p < 0.05$ in Student's *t* test; $n = 3$ blots from three different sets of littermates). (F) Electron microscopic data of the corpus callosum of conditional knockout and control mice at 2 wk following TAM injection are shown. The scale bars indicate 2 µm. (G) Graph of g-ratios of myelinated axons for axon diameters is shown ($n = 448$ axons for three different knockout mice and $n = 469$ axons for their littermate controls). (H) Average g-ratios are shown (*, $p < 0.05$ in Student's *t* test). (I) Graph of the distributions of g-ratios is shown.

composed of 5′-GATCCGTAGAGGCTTATCTCCGTCCTGTGAAGCCACAGATGGGGACGGGGATAAGTCTCTGCTTTTTTACGCGTAT-3′ (sense) and 5′-CGATACGCGTAAAAAAGCAGAGACTTATCCCCGTCCCCATCTGTGGCTTCACAGGACGGAGATAAGCGTCTACG-3′; and the control *Photinus pyralis* luciferase shRNA is composed of 5′-GATCCGGCCATTCTATCCTCTAGACTGTGAAGCCACAGATGGGTCTAGAGGATAGAATGGCCTTTTTTACGCGTAT-3′ (sense) and 5′-CGATACGCGTAAAAAA GGCCATTCTATCCTCTAGACCCATCTGTGGCTTCACAGTCTAGAGGATAGAATGGCCG-3′ (antisense). The annealed duplexes were ligated into the retrovirus vector, pSINmU6 (Takara Bio, Shiga, Japan).

Primary oligodendrocyte cultures

Oligodendrocyte precursor cells were isolated from embryonic day 15 (E15) Sprague Dawley rats (Miyamoto *et al.*, 2007, 2008, 2014b). Briefly, cerebral cortices were dissected, dissociated with 0.25% trypsin, triturated, and passed through mesh with 70 µm pores. Cells were collected, resuspended in MEM containing 10% fetal bovine serum, 50 U/ml penicillin, and 50 µg/ml streptomycin, and seeded on poly-L-lysine–coated dishes. After two passages, the cells were cultured on noncoated Petri dishes (Thermo Scientific). On the second day of culture, the medium was changed to a DMEM-based serum-free growth medium containing the growth factors PDGF and FGF (PDGF-AA and bFGF; Peprotech, Rocky Hill, NJ) and N2

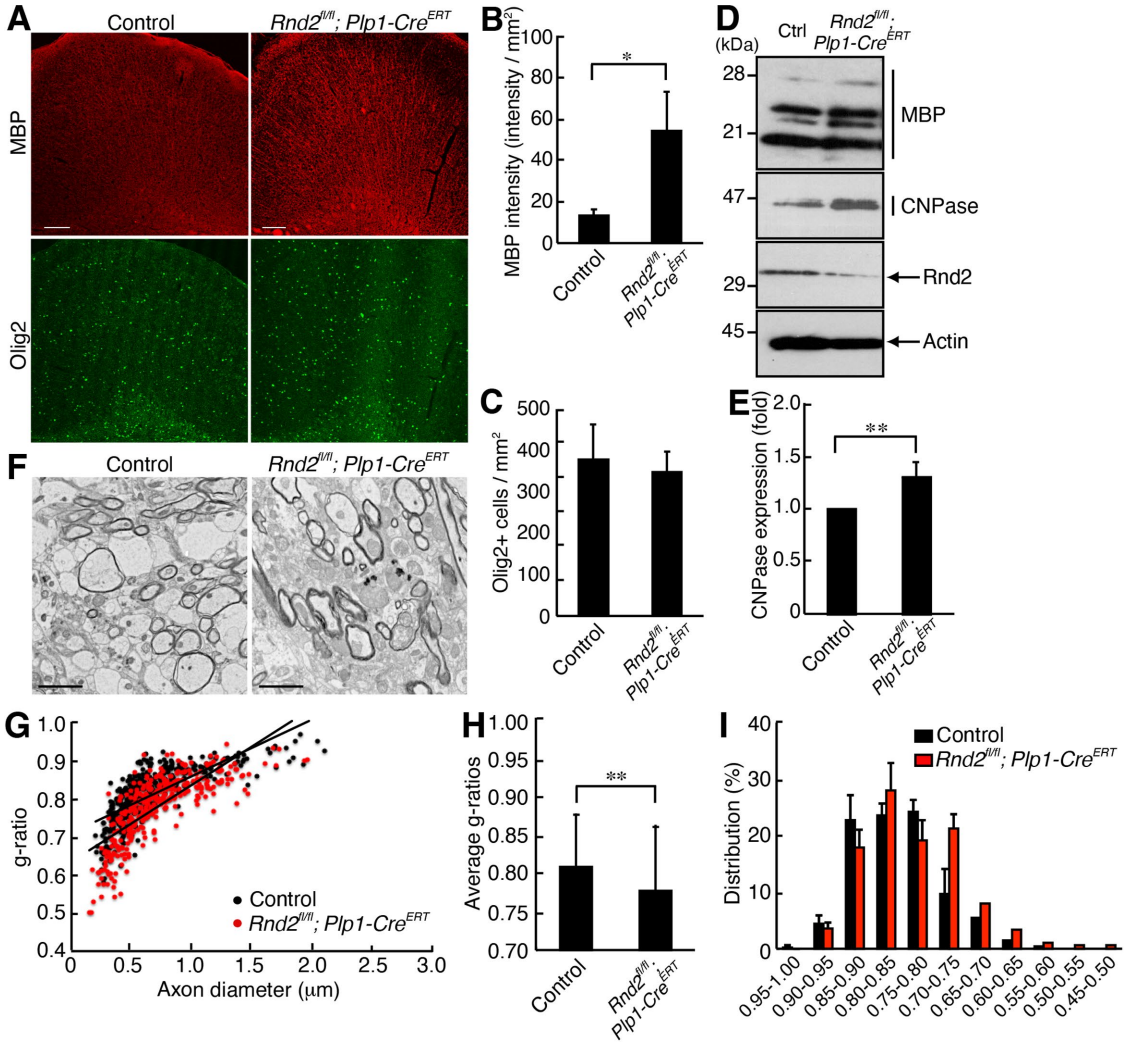

FIGURE 10: Plp1-Cre^{ERT}–mediated Rnd2 knockout mice exhibit increased myelin thickness in adult mice at 4 wk after tamoxifen administration. (A) Eight- or nine-week-old mice were given TAM for 5 consecutive days. Four weeks following the final TAM injection, antibodies against MBP (red) and Olig2 (green) were used for costaining in TAM-treated *Rnd2$^{fl/fl}$; Plp1-Cre^{ERT}* or control mouse brain cross-sections. The scale bars indicate 200 μm. (B) The intensity of MBP staining per square millimeter was relatively semiquantified (*, $p < 0.05$ in Student's *t* test; $n = 6$ sections from three different sets of littermates). (C) The Olig2$^+$ cells per square millimeter were counted ($n = 6$ sections from three different sets of littermates). (D) The brain lysates from TAM-treated Plp1-Cre^{ERT}–driven Rnd2 conditional knockout or control mice were immunoblotted with an antibody against MBP, CNPase, Rnd2, or actin. (E) CNPase expression levels are shown statistically (**, $p < 0.01$ in Student's *t* test; $n = 4$ blots from three different sets of littermates). (F) Electron microscopic data of the corpus callosum of conditional knockout and control mice at 4 wk following TAM injection are shown. The scale bars indicate 2 μm. (G) Graph of g-ratios of myelinated axons for axon diameters is shown ($n = 353$ axons for three different knockout mice and $n = 403$ axons for their littermate controls). (H) Average g-ratios are shown (**, $p < 0.01$ in Student's *t* test). (I) Graph of the distributions of g-ratios is shown.

(Life Technologies), and cells were cultured for an additional 2 d. These cells were then used as oligodendrocyte precursor cells (a proliferating state before differentiation). The isolated cells indeed possessed the oligodendrocyte precursor cell marker PDGF receptor α (GEO accession No. GSE114957; Miyamoto *et al.*, 2016). They also had the oligodendrocyte lineage cell markers Olig1 and Olig2 but not the astrocyte markers Nfia, Sox9, Gfap, and Aqp4 (see Table 1). To induce their differentiation, cells were cultured with a differentiation medium containing 20 ng/ml triodothyronine and 20 ng/ml thyroxine but no growth factor. After 3 d, these cells gradually differentiated into mature oligodendrocytes with MBP-positive myelin web-like structures with myelin markers (see Table 1). To confirm the viability of the attached cells, cells were stained with 0.4% trypan blue. Trypan blue–incorporating cells numbered fewer than 5% in each experiment in this study.

Production of retroviruses and retrovirus-mediated DNA transfection

Using a CalPhos Transfection kit (Takara Bio), each retrovirus vector was cotransfected into G3Thi cells with vectors pVSVG and pGP, which were provided with the Takara Bio retroviral production kit. After 2 d, each culture supernatant was centrifuged at 10,000 rpm for 8 h to concentrate the recombinant retroviruses. The virus pellets were suspended in each culture medium. Because retroviruses are

	MBP expression	CNPase expression	g-ratio	pMBS pRho kinase
P14 Rnd2 KO	↓	↓	↑	↑
P28 Rnd2 KO	↑	↑	↓	↓
P14 Rnd2 Tg	↑	↑	↓	↓
P28 Rnd2 Tg	↓	↓	↑	↑
2 wk after tamoxifen	↓	↓	↑	n. d.
4 wk after tamoxifen	↑	↑	↓	n. d.

n. d. indicates not determined.

TABLE 2: Summary of the increases (↑) and decreases (↓) in experimental values in genetically modified mice compared with controls.

infected into proliferating cells, they were used for transfection (infection) into growing, primary oligodendrocyte precursor cells before being cocultured with neurons (Miyamoto *et al.*, 2008, 2014b).

Oligodendrocyte-neuronal cocultures

DRG neurons, whose axons are generally connected from peripheral tissues to the CNS via the spinal cord, were isolated from E15 Sprague Dawley rats and then dissociated and plated onto collagen (type I)-coated 22-mm coverslips (Chan *et al.*, 2004; Yamauchi *et al.*, 2012; Miyamoto *et al.*, 2013). Nonneuronal growing cells were eliminated by cycling three times with medium containing 5-fluorodeoxyuridine and uridine. Cocultures were established by seeding ~200,000 purified oligodendrocyte precursor cells on neurons. Cocultures were maintained for 3–4 wk. Medium was replaced every 3–4 d.

Immunoblotting

Tissues or cells were lysed in lysis buffer (50 mM HEPES-NaOH [pH 7.5], 20 mM $MgCl_2$, 150 mM NaCl, 1 mM dithiothreitol, 1 mM phenylmethane sulfonylfluoride, 1 μg/ml leupeptin, 1 mM EDTA, 1 mM Na_3VO_4, 10 mM NaF, 0.5% NP-40, 1% CHAPS, and 0.1% or 0.3% SDS) to elute myelin segment proteins and were centrifuged in a microcentrifuge to obtain clear supernatants (Chan *et al.*, 2004; Yamauchi *et al.*, 2012; Miyamoto *et al.*, 2013, 2018). These lysates (10 μg per sample on average) were denatured and subjected into SDS–polyacrylamide gels. The electrophoretically separated proteins were transferred to a polyvinylidene difluoride membrane, blocked with Blocking One reagent (Nacalai Tesque, Kyoto, Japan), and immunoblotted first with primary antibodies and then with peroxidase-conjugated secondary antibodies. The bound antibodies were detected using a normal- or high-sensitivity chemiluminescence detection kit (FUJIFILM Wako Pure Chemical Corporation, Tokyo, Japan). Littermate mice (genetically modified mice and control mice) were harvested on different days, and at least three sets were prepared for experiments. All photos in the figures are representative of multiple experiments.

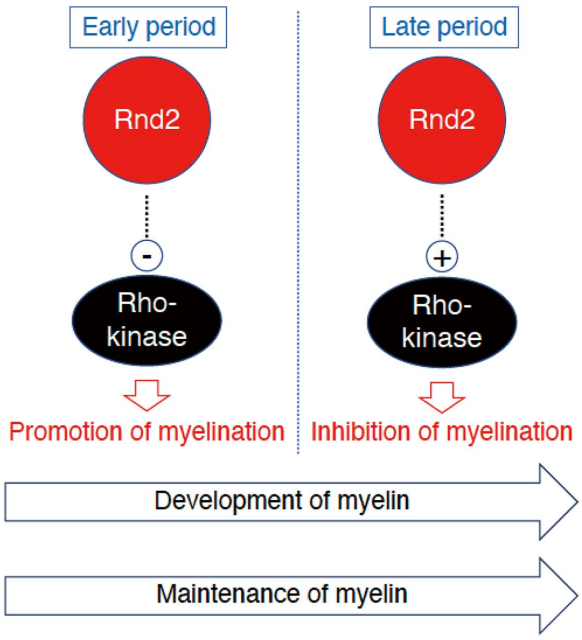

FIGURE 11: Schematic diagram of the role of Rnd2 in myelination. In earlier myelinating periods, Rnd2 down-regulates Rho kinase to promote myelination. In later myelinating periods, Rnd2 up-regulates Rho kinase to inhibit myelination.

Immunofluorescence

Cells on coverslips or dishes were normally fixed with 4% paraformaldehyde (PFA). Four percent PFA followed by 100% cold methanol was used for myelin segment staining (Chan *et al.*, 2004; Yamauchi *et al.*, 2012; Miyamoto *et al.*, 2013, 2018). Cells were permeabilized with phosphate-buffered saline (PBS) containing 0.1% Triton X-100, blocked with Blocking One reagent, and incubated first with primary antibodies and then with fluorescence-labeled secondary antibodies. The coverslips or dishes were mounted with Vectashield reagent with 4′,6-diamidino-2-phenylindole (DAPI; Vector Laboratories, Burlingame, CA). The fluorescence images were captured with a DMI4000B fluorescence microscope system (Leica, Wetzlar, Germany) and analyzed with AF6000 software (Leica). Culture dishes (Rnd2 shRNA and control shRNA) were harvested on different days, and at least three sets were prepared for experiments. All photos in the figures are representative of multiple experiments.

Immunohistochemistry

Tissues were perfused first with PBS and then with PBS containing 4% PFA. The tissues were postfixed with 4% PFA, replaced with 20% sucrose, and embedded in Tissue-Tek reagent (Sakura Finetechnical, Tokyo, Japan) (Chan *et al.*, 2004; Yamauchi *et al.*, 2012; Miyamoto *et al.*, 2013, 2018). The cryosections for immunostaining with an antibody for O4 were prepared according to the manufacturer's instructions (Merck-Millipore). Microtome sections on glass slides were blocked with Blocking One reagent and incubated first with primary antibodies and then with fluorescence-labeled secondary antibodies. The glass slides were mounted with Vectashield reagent. The fluorescent images were collected with an IX81 microscope system (Olympus, Tokyo, Japan) equipped with a laser-scanning FV500 or FV1000D

(Olympus) and analyzed with Fluoview software (Olympus). Littermate mice (genetically modified mice and control mice) were harvested on different days, and at least three sets were prepared for experiments. All photos in the figures are representative of multiple experiments.

Electron microscopy

Tissues were fixed with 2% PFA and 2% glutaraldehyde in 0.1% cacodylate-containing buffer. They were then contrasted with 2% osmium tetroxide, dehydrated with an ethanol gradient, and treated with propylene oxide. Finally, samples were infiltrated and embedded in pure epoxy resin. Ultrathin sections were stained with uranyl acetate and lead staining solution. Images were taken with a JEM-1200EX or JEM-1400 Plus electron microscope system (JOEL, Tokyo, Japan) by the Hana-ichi Ultrastructure Research Institute (Nagoya, Japan). The g-ratio is the ratio of the diameter of the axon proper (i.e., not including any myelin) to the outer diameter of the myelinated axon. These ratios were plotted to determine axon diameter. Their distributions are also shown in the graph.

Transcriptome analysis

We previously registered data for primary rat oligodendroglial precursor cell mRNAs before (day 0) and after (day 3) the induction of differentiation (GEO Acc. No. GSE114957; Miyamoto *et al*., 2016). Briefly, total RNA was labeled with Cy5 using an Amino Allyl MessageAMP II aRNA Amplification Kit (Thermo Fisher Scientific). A 3D-Gene chip (rat oligo chip 20k; Toray, Tokyo, Japan) was used for microarray analysis by the Toray 3D-Gene chip service (URL: http://www.3d-gene.com/). The signals, which were hybridized to Cy5-labeled RNA pools, were obtained using a Toray 3D-Gene scanner. The detected signals for the respective genes were normalized according to the global normalization method and were processed by the Kamakura-Techno 3D-Gene analytical service (URL: http://www.kamakura-ts.co.jp/). The median value of the detected signal intensities was adjusted to 25. Values greater than 100 were considered valid.

Statistical analysis

Values shown in the figure panels represent the means ± SD from separate experiments. Comparisons between two experimental groups were made using Student's *t* test (**, $p< 0.01$, *, $p< 0.05$). A one-way analysis of variance (ANOVA) was followed by a Fisher's protected least significant difference (PLSD) test as a post hoc comparison (**, $p < 0.01$, *, $p < 0.05$).

Animal studies

Genetically modified/unmodified mice were handled in accordance with a protocol approved by the Japanese National Research Institute for Child Health and Development Animal Care Committee. Gene recombination processes were handled in accordance with a protocol approved by the Japanese National Research Institute for Child Health and Development Gene Recombination Committee.

ACKNOWLEDGMENTS

This work was supported by Grants-in-Aid for Scientific Research from the Japanese Ministry of Education, Culture, Sports, Science and Technology (MEXT), for Medical Scientific Research from the Japanese Ministry of Health, Labor, and Welfare (MHLW), and from The Naito Foundation. This work was also supported by the Takeda Science Foundation. We acknowledge Chris Rowthorn Japan (Kyoto, Japan) for proofreading.

REFERENCES

Bennett MR, Rizvi TA, Karyala S, McKinnon RD, Ratner N (2003). Aberrant growth and differentiation of oligodendrocyte progenitors in neurofibromatosis type 1 mutants. J Neurosci 23, 7207–7217.

Bergles DE, Richardson WD (2015). Oligodendrocyte development and plasticity. Cold Spring Harb Perspect Biol 8, a020453.

Bradl M, Lassmann H (2010). Oligodendrocytes: biology and pathology. Acta Neuropathol 119, 37–53.

Chan JR, Watkins TA, Cosgaya JM, Zhang C, Chen L, Reichardt LF, Shooter EM, Barres BA (2004). NGF controls axonal receptivity to myelination by Schwann cells or oligodendrocytes. Neuron 43, 183–191.

Chardin P (2006). Function and regulation of Rnd proteins. Nat Rev Mol Cell Biol 7, 54–62.

Devreotes P, Horwitz AR (2015). Signaling networks that regulate cell migration. Cold Spring Harb Perspect Biol 7, a005959.

Dugas JC, Tai YC, Speed TP, Ngai J, Barres BA (2006). Functional genomic analysis of oligodendrocyte differentiation. J Neurosci 26, 10967–10983.

Foster R, Hu KQ, Lu Y, Nolan KM, Thissen J, Settleman J (1996). Identification of a novel human Rho protein with unusual properties: GTPase deficiency and in vivo farnesylation. Mol Cell Biol 16, 2689–2699.

Fujita H, Katoh H, Ishikawa Y, Mori K, Negishi M (2002). Rapostlin is a novel effector of Rnd2 GTPase inducing neurite branching. J Biol Chem 277, 45428–45434.

Goebbels S, Oltrogge JH, Kemper R, Heilmann I, Bormuth I, Wolfer S, Wichert SP, Möbius W, Liu X, Lappe-Siefke C, *et al*. (2010). Elevated phosphatidylinositol 3,4,5-trisphosphate in glia triggers cell-autonomous membrane wrapping and myelination. J Neurosci 30, 8953–8964.

Heng JI, Nguyen L, Castro DS, Zimmer C, Wildner H, Armant O, Skowronska-Krawczyk D, Bedogni F, Matter JM, Hevner R, *et al*. (2008). Neurogenin 2 controls cortical neuron migration through regulation of Rnd2. Nature 455, 114–118.

Jaffe AB, Hall A (2005). Rho GTPases: biochemistry and biology. Annu Rev Cell Dev Biol 21, 247–269.

Liang X, Draghi NA, Resh MD (2004). Signaling from integrins to Fyn to Rho family GTPases regulates morphologic differentiation of oligodendrocytes. J Neurosci 24, 7140–7149.

Mi S, Lee X, Shao Z, Thill G, Ji B, Relton J, Levesque M, Allarie N, Perrin S, Sands B, *et al*. (2004). LINGO-1 is a component of the Nogo-66 receptor/p75 signaling complex. Nat Neurosci 7, 221–228.

Miyamoto Y, Torii T, Eguchi T, Nakamura K, Tanoue A, Yamauchi J (2014a). Hypomyelinating leukodystrophy-associated missense mutant of FAM126A/hyccin/DRCTNNB1A aggregates in the endoplasmic reticulum. J Clin Neurosci 21, 1033–1039.

Miyamoto Y, Torii T, Tago K, Tanoue A, Takashima S, Yamauchi J (2018). BIG1/Arfgef1 and Arf1 regulate the initiation of myelination by Schwann cells in mice. Sci Adv 4, eaar4471.

Miyamoto Y, Torii T, Tanoue A, Yamauchi J (2016). VCAM1 acts in parallel with CD69 and is required for the initiation of oligodendrocyte myelination. Nat Commun 7, 13478.

Miyamoto Y, Torii T, Yamamori N, Tanoue A, Yamauchi J (2013). Akt and PP2A reciprocally regulate the guanine nucleotide exchange factor Dock6 to control axon growth of sensory neurons. Sci Signal 6, ra15.

Miyamoto Y, Yamamori N, Torii T, Tanoue A, Yamauchi J (2014b). Rab35, acting through ACAP2 switching off Arf6, negatively regulates oligodendrocyte differentiation and myelination. Mol Biol Cell 25, 1532–1542.

Miyamoto Y, Yamauchi J, Chan JR, Okada A, Tomooka Y, Hisanaga S, Tanoue A (2007). Cdk5 regulates differentiation of oligodendrocyte precursor cells through the direct phosphorylation of paxillin. J Cell Sci 120, 4355–4366.

Miyamoto Y, Yamauchi J, Tanoue A (2008). Cdk5 phosphorylation of WAVE2 regulates oligodendrocyte precursor cell migration through nonreceptor tyrosine kinase Fyn. J Neurosci 28, 8326–8337.

Nawaz S, Sánchez P, Schmitt S, Snaidero N, Mitkovski M, Velte C, Brückner BR, Alexopoulos I, Czopka T, Jung SY, *et al*. (2015). Actin filament turnover drives leading edge growth during myelin sheath formation in the central nervous system. Dev Cell 34, 139–151.

Pacary E, Heng J, Azzarelli R, Riou P, Castro D, Lebel-Potter M, Parras C, Bell DM, Ridley AJ, Parsons M, *et al*. (2011). Proneural transcription factors regulate different steps of cortical neuron migration through Rnd-mediated inhibition of RhoA signaling. Neuron 69, 1069–1084.

Riou P, Villalonga P, Ridley AJ (2010). Rnd proteins: multifunctional regulators of the cytoskeleton and cell cycle progression. Bioessays 32, 986–992.

Rossman KL, Der CJ, Sondek J (2005). GEF means go: turning on RHO GTPases with guanine nucleotide exchange factors. Nat Rev Mol Cell Biol 6, 167–180.
Saab AS, Nave KA (2017). Myelin dynamics: protecting and shaping neuronal functions. Curr Opin Neurobiol 47, 104–112.
Sanz-Rodriguez M, Gruart A, Escudero-Ramirez J, de Castro F, Delgado-Garcia JM, Wandosell F, Cubelos B (2018). R-Ras1 and R-Ras2 are essential for oligodendrocyte differentiation and survival for correct myelination in the central nervous system. J Neurosci 38, 5096–5110.
Simons M, Lyons DA (2013). Axonal selection and myelin sheath generation in the central nervous system. Curr Opin Cell Biol 25, 512–519.
Snaidero N, Velte C, Myllykoski M, Raasakka A, Ignatev A, Werner HB, Erwig MS, Möbius W, Kursula P, Nave KA, Simons M (2017). Antagonistic functions of MBP and CNP establish cytosolic channels in CNS myelin. Cell Rep 18, 314–323.
Tanaka H, Katoh H, Negishi M (2006). Pragmin, a novel effector of Rnd2 GTPase, stimulates RhoA activity. J Biol Chem 281, 10355–10364.
Thurnherr T, Benninger Y, Wu X, Chrostek A, Krause SM, Nave KA, Franklin RJ, Brakebusch C, Suter URelvas JB (2006). Cdc42 and Rac1 signaling are both required for and act synergistically in the correct formation of myelin sheaths in the CNS. J Neurosci 26, 10110–10119.
Wennerberg K, Forget MA, Ellerbroek SM, Arthur WT, Burridge K, Settleman J, Der CJ, Hansen SH (2003). Rnd proteins function as RhoA antagonists by activating p190 RhoGAP. Curr Biol 13, 1106–1115.
Yamauchi J, Miyamoto Y, Torii T, Takashima S, Kondo K, Kawahara K, Nemoto N, Chan JR, Tsujimoto G, Tanoue A (2012). Phosphorylation of cytohesin-1 by Fyn is required for initiation of myelination and the extent of myelination during development. Sci Signal 5, ra69.
Zhao XH, Jin WL, Ju G (2007). An in vitro study on the involvement of LINGO-1 and Rho GTPases in Nogo-A regulated differentiation of oligodendrocyte precursor cells. Mol Cell Neurosci 36, 260–269.
Zou Y, Jiang W, Wang J, Li Z, Zhang J, Bu J, Zou J, Zhou L, Yu S, Cui Y, *et al.* (2014). Oligodendrocyte precursor cell-intrinsic effect of Rheb1 controls differentiation and mediates mTORC1-dependent myelination in brain. J Neurosci 34, 15764–15778.
Zuchero JB, Barres BA (2013). Intrinsic and extrinsic control of oligodendrocyte development. Curr Opin Neurobiol 23, 914–920.
Zuchero JB, Fu MM, Sloan SA, Ibrahim A, Olson A, Zaremba A, Dugas JC, Wienbar S, Caprariello AV, Kantor C, *et al.* (2015). CNS myelin wrapping is driven by actin disassembly. Dev Cell 34, 152–167.